JGP Journal of General Physiology

ARTICLE

Enhancing diastolic function by strain-dependent detachment of cardiac myosin crossbridges

Bradley M. Palmer[1], Douglas M. Swank[2], Mark S. Miller[3], Bertrand C.W. Tanner[4], Markus Meyer[5], and Martin M. LeWinter[5]

The force response of cardiac muscle undergoing a quick stretch is conventionally interpreted to represent stretching of attached myosin crossbridges (phase 1) and detachment of these stretched crossbridges at an exponential rate (phase 2), followed by crossbridges reattaching in increased numbers due to an enhanced activation of the thin filament (phases 3 and 4). We propose that, at least in mammalian cardiac muscle, phase 2 instead represents an enhanced detachment rate of myosin crossbridges due to stretch, phase 3 represents the reattachment of those same crossbridges, and phase 4 is a passive-like viscoelastic response with power-law relaxation. To test this idea, we developed a two-state model of crossbridge attachment and detachment. Unitary force was assigned when a crossbridge was attached, and an elastic force was generated when an attached crossbridge was displaced. Attachment rate, $f(x)$, was spatially distributed with a total magnitude f_0. Detachment rate was modeled as $g(x) = g_0 + g_1x$, where g_0 is a constant and g_1 indicates sensitivity to displacement. The analytical solution suggested that the exponential decay rate of phase 2 represents ($f_0 + g_0$) and the exponential rise rate of phase 3 represents g_0. The depth of the nadir between phases 2 and 3 is proportional to g_1. We prepared skinned mouse myocardium and applied a 1% stretch under varying concentrations of inorganic phosphate (Pi). The resulting force responses fitted the analytical solution well. The interpretations of phases 2 and 3 were consistent with lower f_0 and higher g_0 with increasing Pi. This novel scheme of interpreting the force response to a quick stretch does not require enhanced thin-filament activation and suggests that the myosin detachment rate is sensitive to stretch. Furthermore, the enhanced detachment rate is likely not due to the typical detachment mechanism following MgATP binding, but rather before MgADP release, and may involve reversal of the myosin power stroke.

Introduction

Muscle performance is often gauged in terms of contractile force and power. The capacity to relax and relengthen is also critical to the function of many muscle types. Cardiac muscle, for example, must relengthen during the diastolic phase of the cardiac cycle to ensure adequate ventricular chamber filling. A slowed or partially completed filling of the left ventricle (LV) is a pathophysiologic mechanism underlying ≥50% of all cases of heart failure and is a growing societal health concern (Dunlay et al., 2017). One factor affecting diastolic function is the force-producing myosin enzyme, which will inhibit relengthening if still attached to actin as diastole progresses.

The most influential determinant of myosin detachment from actin is the rate-limiting MgADP release step. A slower MgADP release rate, as occurs in the cardiac β-myosin isoform compared with α-myosin, for example, prolongs the lifetime of the force-producing myosin crossbridge (Tyska and Warshaw, 2002). The longer-lived crossbridge, in turn, slows the decay of muscle contractile force during relaxation and thereby would be expected to inhibit myocardial lengthening in diastole (Kass et al., 2004). The MgADP release rate is also slowed when a resistive load, as occurs with muscle lengthening, is applied to the myosin crossbridge (Veigel et al., 2005; Kad et al., 2007; Liu et al., 2018). These two factors, the predominance of β-myosin isoform in the human LV and the strain-dependent slowing of MgADP release during myocardial lengthening, work against myocardial relengthening and diastolic function.

Conversely, mechanisms within the myofilaments that enhance the crossbridge detachment rate in response to stretch would benefit diastolic function by reducing the mechanical energy required to lengthen the myocardium. One possibility is an additional, faster crossbridge detachment pathway before MgADP release, perhaps coincident with rebinding of inorganic phosphate (Pi). A Pi-dependent crossbridge detachment before MgADP release has been shown to be facilitated by a resistive

[1]Department of Molecular Physiology and Biophysics, University of Vermont, Burlington, VT; [2]Department of Biological Sciences and Biomedical Engineering Center for Biotechnology and Interdisciplinary Studies, Rensselaer Polytechnic Institute, Troy, NY; [3]Department of Kinesiology, University of Massachusetts-Amherst, Amherst, MA; [4]Department of Integrative Physiology and Neuroscience, Washington State University, Pullman, WA; [5]Department of Medicine, University of Vermont, Burlington, VT.

Correspondence to Bradley M. Palmer: bmpalmer@uvm.edu.

load as occurs with muscle lengthening (Dantzig et al., 1992; Smith and Geeves, 1995) and, therefore, could play a role in decreasing resistance during myocardial lengthening. Such a mitigation of cardiac force during lengthening has been reported in intact myocardium undergoing stretch in late systole (Chung et al., 2017).

The idea that myosin crossbridges are more likely to detach during stretch suggests an alternative interpretation of the experimentally observed force response to a quick stretch. The current prevailing interpretation includes an enhancement of thin filament activation with stretch, frequently referred to as stretch activation (Campbell, 1997; Campbell and Chandra, 2006). We would argue that, because cardiac muscle retains the familiar force response to a quick stretch even after removal of thin-filament regulatory proteins (Kawai and Ishiwata, 2006), the typical features of the force response to stretch in cardiac muscle do not rely on effects of thin-filament regulatory proteins. Our proposed enhancement of detachment rate with stretch does not focus on any strain effects on MgADP release rate, but rather on some other strain-dependent pathway possibly involving Pi rebinding (Smith and Geeves, 1995). In this paper, we present the basis of a hypothesis that a strain-dependent enhancement of the myosin crossbridge detachment rate underlies the salient features of the force response to stretch.

Materials and methods

Solutions

Chemicals and reagents were obtained from Sigma-Aldrich unless otherwise noted. Krebs solution contained (in mmol/liter) 127 NaCl, 2 KCl, 1.3 KH_2PO_4, 2.5 $CaCl_2$, 0.6 $MgSO_4$, 25 $NaHCO_3$, and 10 glucose, pH 7.4; nonactivating solution: calcium concentration (pCa) 8.0, 5 EGTA, 5 MgATP, 1 Mg^{2+}, 0–8 Pi, 35 phosphocreatine, and 300 U/ml creatine kinase, ionic strength 200, pH 7.0; activating solution: same as nonactivating, with pCa 4.0; rigor solution: same as relaxing, with pCa 4.8 and 0 MgATP; skinning solution: same as relaxing, without creatine kinase and with 1% Triton X-100 wt/vol, 10 µl/ml E-64, 1.25 µl/ml PMSF, 1 tablet/10 ml PhosStop phosphatase inhibitor cocktail, and 50% glycerol wt/vol; storage solution: same as skinning, without Triton X-100. Where indicated, the myosin crossbridge inhibitor 2,3-butanedione 2-monoxime (BDM) was added at 40 mM.

Mouse myocardium

All procedures were reviewed and approved by the Institutional Animal Care and Use Committee of the University of Vermont College of Medicine and complied with Guide for the Use and Care of Laboratory Animals published by the National Institutes of Health. Animals were fully anesthetized with isoflurane and hearts were removed. Papillary muscles from the LV were isolated, removed, and placed in preoxygenated (95% O_2, 5% CO_2) Krebs-Ringer solution at room temperature and demembranated overnight at 4°C in skinning solution. Skinned myocardial strips were prepared and studied as previously described (Donaldson et al., 2012; Zile et al., 2015). Strips were mounted between a piezoelectric motor (P841.60, Physik Instrumente) and a strain gauge (AE801, Kronex), lowered into a 30-µl droplet of relaxing solution maintained at 17°C, and stretched to 2.2 µm sarcomere length (IonOptix). Strips were subjected to activating and rigor solutions to induce distinct experimental conditions. Force responses were recorded after step-length changes of 0.25, 0.5, or 1.0% resting muscle length (ML). In some cases, constant velocities were imposed at 1, 0.5, 0.2, 0.1, and 0.05 ML/s, which corresponded to 1% ML change over 10, 20, 50, and 100 ms.

Human myocardium

All patients signed informed consent forms approved by the University of Vermont Institutional Review Board. LV epicardial biopsies were obtained during coronary bypass graft procedures as described previously (Donaldson et al., 2012; Zile et al., 2015). Skinned strips were prepared and examined as described for mouse myocardium above but at 37°C.

Computer simulations

Computer simulations were performed using IDL v8.4 (Exelis Visual Information Solutions). The status of a single myosin head was modeled to alternate between a non–force-producing detached (D) state and a force-producing attached (A) state. A period of 1.1 s was simulated and broken into increments of equal duration, $t_{inc} = 10^{-4}$ s. When the myosin head was in the D state, the probability of transitioning to the A state within t_{inc} was calculated as $1 - \exp(-f_0 \times t_{inc})$, where f_0 = attachment rate in units of s^{-1}. The transition at any time increment occurred when a uniformly distributed random number, n, generated in the range $0 \le n < 1$ was less than the calculated transition probability. Upon transitioning from D to A, an initial displacement x_{init} was randomly generated according to a Gaussian distribution with 0 mean and 5 nm SD and assigned to the myosin head. This initial displacement was then apprised with each time increment according to the simulated length change of the half-sarcomere so that displacement of the myosin head $x = x_{init} + L(t)$. For quick stretch length changes, maximum length change was 10 nm or 1% of a 1.0-µm half-sarcomere over 2 ms. When the myosin head was in the A state, the probability of transitioning to D within t_{inc} was calculated as $1 - \exp[-(g_0 + g_1 x) \times t_{inc}]$, where g_0 = detachment rate in s^{-1} and g_1 = sensitivity of detachment rate to crossbridge displacement in $s^{-1} \cdot nm^{-1}$. All spatial displacements and probabilities were characterized with double-precision floating point variables.

The simulated force for any one crossbridge looks like the result of a laser trap experiment in which unitary force and deflection of force due to strain can be recorded experimentally. 5 million of these crossbridges were simulated and added together for one simulated half-sarcomere force response to the length change. Statistics such as mean displacement $A_1(t)$ and fraction attached $A_0(t)$ were recorded. Values for the parameters f_0, g_0, and g_1 were varied to test the validity and limits of the above analytical solutions for $A_1(t)$ and $A_0(t)$ to represent the outcomes of the simulations. Other parameters used in the simulations were the number of possible myosin crossbridges in the half-sarcomere $N_{hs} = 10^{13}$, length of the half-sarcomere L_{hs} = 1,000 nm, cross-sectional area (CSA) = 1 mm^2, stiffness of a

myosin crossbridge k_{stiff} = 1 pN · nm^{-1}, and unitary force of myosin crossbridge F_{uni} = 10 pN, which corresponded to

$$\frac{N_{hs}F_{uni}}{CSA} = 10 \text{ mN} \cdot \text{mm}^{-2}$$

and

$$\frac{L_{hs}N_{hs}k_{stiff}}{CSA} = 10 \text{ mN} \cdot \text{mm}^{-2}.$$

The orders of magnitude for these values were based on findings reported from measurements made in single molecules (Tyska and Warshaw, 2002) but are not intended to strictly reflect the only possible values for these parameters.

Fitting mathematical model to recorded data

Each step force response, either recorded or simulated, was baseline subtracted and fitted to the dynamic terms of Eq. 7 using a Levenberg–Marquardt nonlinear least-squares fit. Estimates were made of six parameters defined later in the text:

$$\left(L_{hs}\gamma\frac{g_1\bar{A}_0}{f_0}\right),\ (L_{hs}\lambda\bar{A}_0),\ (f_0 + g_0),\ g_0,\ G_p, \text{ and } k_p.$$

To reduce issues related to starting guesses and covariance among parameter estimates, values for G_p and k_p were estimated first using time points greater than the time point of phase 3 peak and were then held constant for the fitting of the remaining four parameters using time points >5 ms. Finally, all six parameters were fitted for time points >5 ms to refine final parameter estimates.

Supplemental derivation of mathematical model

The conceptual model described above lends itself to an analytical solution. The derivation and explicit assumptions that lead to the analytical solution are presented in the Supplemental text (see bottom of PDF). The results of the model are presented in the text below.

Online supplemental material

Supplemental text presents the derivation and explicit assumptions that led to the analytical solution.

Results

Interpretations of the force response to a step-length change

Characteristics of myofilament function in striated muscle are often assessed in vitro by recording tensile force measured at one end of a muscle strip preparation in response to a quick step-length change applied at the other end (Fig. 1 A and inset). After normalizing force to cross-sectional area and length to resting ML, the change in stress caused by the imposed strain characterizes the dynamic stiffness, i.e., viscoelasticity, of the muscle. A typical step force response in submaximally Ca^{2+}-activated demembranated human myocardium is shown in Fig. 1 B. It has been suggested that the instantaneous force rise (phase 1), then rapid force decay (phase 2), followed by a slowly rising (phase 3) and elevated (phase 4) force are due to stretching of attached myosin crossbridges (phase 1) and detachment of these stretched crossbridges at an exponential decay rate (phase 2), followed by crossbridges reattaching but in increased numbers due to an enhanced activation of the thin filament (phases 3 and 4; Campbell, 1997; Campbell and Chandra, 2006). These measures are often conducted at a sarcomere length that maximizes the overlap of the thick and thin filaments, such as 2.2 µm used here, thereby optimizing any interfilament interaction.

Under relaxed conditions (pCa 8 + BDM), when no force-producing crossbridges are formed, the force response consists solely of an elevated force akin to phase 4 (Fig. 1 C), as would be expected from a passive viscoelastic material. This change in stress observed in the relaxed response of Fig. 1 C is expected to be present when the muscle is activated. When we subtract the stress of the relaxed condition from that of the activated condition, the crossbridge-dependent response (Fig. 1 D) drops below the prestretch isometric tension during phase 2. We argue that the nadir of phase 2 must be due to a transient drop in the number of force-producing crossbridges.

Our argument starts with consideration of phase 4 of activated muscle, which demonstrates a passive-like viscoelastic response bearing a magnitude proportional to the number of attached crossbridges. Fig. 2 A illustrates step force responses in maximally Ca^{2+}-activated conditions (pCa 4.8) and with varying MgATP concentrations. In rigor (i.e., <0.01 mM MgATP), the force response reflects all the available myosin crossbridges formed and contributing to a power-law relaxation commonly found in passive biological tissues (Djordjević et al., 2003). The power-law relaxation of stress in response to a length step is described as Gt^{-k}, where G = stress magnitude in units mN · mm^{-2}, t = time, and k = dimensionless constant $0 < k < 1$ that dictates the relaxation dynamics. Note that magnitude G indicates the change in stress recorded at t = 1 s. Except for some noise spikes, the fit of the recorded stress under rigor conditions to the power-law was within 2% error (Fig. 2 B). The best fit of an exponential function, $ae^{-bt} + c$, was not as good. The power-law fit under relaxed conditions was also generally within 2% error (Fig. 2 B). With these results, we accept that a power-law relaxation reasonably describes the step force response of muscle when myosin crossbridges are not cycling.

We then asked if a power-law relaxation model could reasonably underlie phase 4 when myosin crossbridges are cycling. If so, the magnitude G describing phase 4, which can be quantified as the force recorded at t = 1 s, would be proportional to the myosin crossbridge number and duty cycle. We found that the activated stress response at 1 s above the BDM response is reduced as MgATP rises. When normalized to the total range of stresses between BDM and rigor conditions, the activated response at 1 s above the BDM stress response reaches a steady-state value of <20% when MgATP is at saturating concentrations (Fig. 2 A, inset). While we have not accounted for differences in crossbridge stiffness due to the presence or absence of nucleotide, these observations with varying MgATP are consistent with an expected reduction in myosin crossbridge duty ratio with increasing MgATP. We also found that higher pCa values led to higher values for magnitude G (Fig. 2 C). When normalized, magnitude G displayed a sigmoidal response with calcium

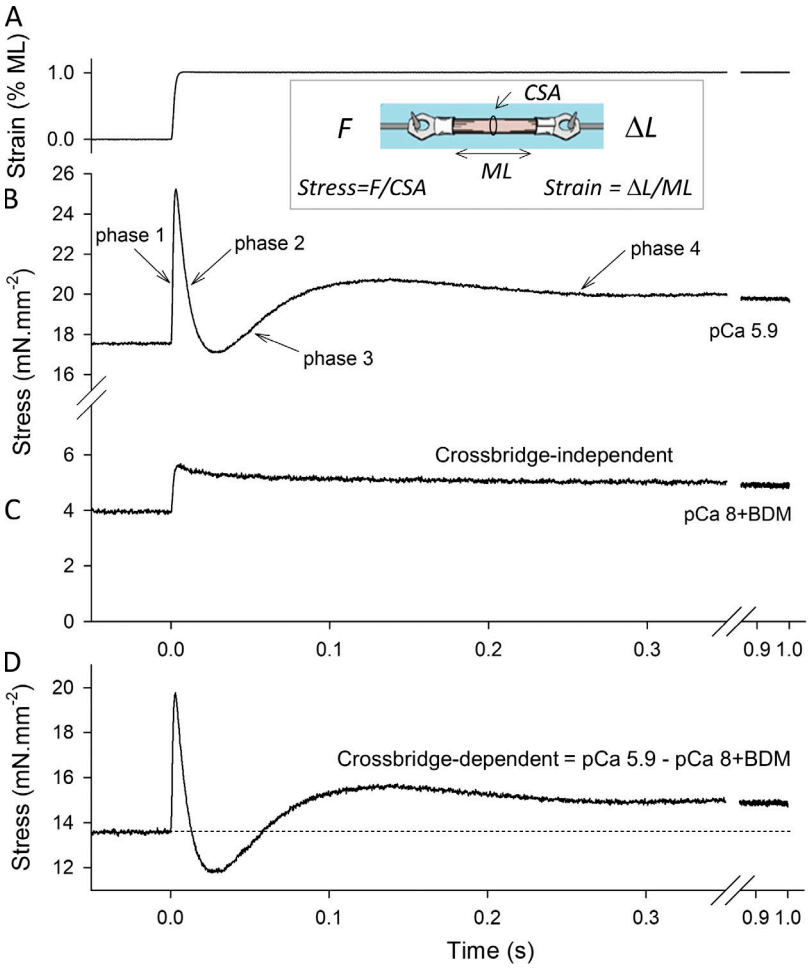

Figure 1. **Example force response to a quick stretch. (A)** This assay entails the application of a step-length change on the order of <1% resting ML. In this example, the ML between the clips (inset) was 310 µm, and a step-length change (Δ*L*) of 3.1 µm was applied and normalized to ML to provide strain. Force (*F*) was recorded and normalized to *CSA* to provide stress. More than 95% of the length step was achieved in <4 ms, and thus was considered a quick stretch. **(B)** At submaximal Ca^{2+} activation, the step force response of skinned human myocardium displays the four phases typically observed. These phases are most often attributed to the stretch of attached myosin crossbridges (phase 1) and gradual detachment of the stretched crossbridges (phase 2), followed by enhanced thin filament activation resulting in a gradual rise (phase 3) and maintenance (phase 4) of an elevated force. **(C)** An elevated force is also observed under relaxed conditions with no myosin crossbridges formed, i.e., pCa 8 + BDM. The change in stress associated with this relaxed response would be expected to accompany the activated response. **(D)** The crossbridge-dependent response is calculated here as the activated recording minus the relaxed recording. The resulting crossbridge-dependent stress after stretch dips below the prestretch stress for a short period between phases 2 and 3. We propose that a transient depression of contractile force underlies the nadir of phases 2 and 3.

activation like that of isometric tension (Fig. 2 C, inset). The power-law fit to the force responses under the various calcium activation conditions was within 4% error after 150 ms (Fig. 2 D). We believe it reasonable to consider phase 4 as the tail of a viscoelastic response typical of biological materials and bearing power-law relaxation with magnitude proportional to cross-bridge number. Phases 2 and 3 would then reasonably represent a transient depression of force due to transient reduction in the number of force-producing myosin crossbridges.

Linearity of force response in mouse myocardium

Much of our upcoming argument is based on the premise that the force response to a stretch represents a linear system, which we demonstrate here. The two properties of the force response that demonstrate linearity are homogeneity (i.e., a change of length scales proportionally to the change of force) and additivity (i.e., multiple length changes result in the addition of the respective individual force responses). Linearity occurs, or is at least reasonably approximated, in nonlinear systems with small perturbations. We undertake here a test of a linear response for a quick stretch as well as for slower stretches up to 1% ML.

To demonstrate homogeneity, we compared the scaled responses of different length changes. Step-length changes of 0.25, 0.5, and 1.0% ML were used in these tests (Fig. 3 A). Under relaxed conditions of pCa 8 + BDM, the respective force responses were multiplied by 4, 2, and 1 and superimposed for comparison in Fig. 3 B. Except in the first 10 ms of the response, these relaxed force responses did not differ >2%. At half-maximal calcium activation pCa 5.9, the scaled force responses were superimposed (Fig. 3 C), but some differences can be seen past 10 ms. The errors in the two scaled responses corresponding to 0.25 and 0.5% length changes relative to the 1.0% response were calculated as the difference (scaled response minus 1.0% response) divided by the 1.0% force response at 1 s. Fig. 3 D illustrates that the error was <5% at almost all time points. These results suggest that the property of homogeneity is reasonably approximated to within 5% error.

To demonstrate additivity, we tested if a convolution integral applied to the step length would produce a theoretical force response similar to an actual force response. Fig. 3 E illustrates a step-length change of 1% ML (dashed line) and four ramp length changes to 1% ML over 10, 20, 50, and 100 ms (solid lines), respectively. The first derivatives of the step and of each ramp were compared to each other, resulting in a convolution kernel (Fig. 3 E, inset), which when convolved with the original length step reproduces the ramp. That same kernel was then convolved with the step force response to produce a theoretical force response to the ramp.

The additivity test when the muscle is not activated at pCa 8 + BDM suggests linearity (Fig. 3 F). The original step force

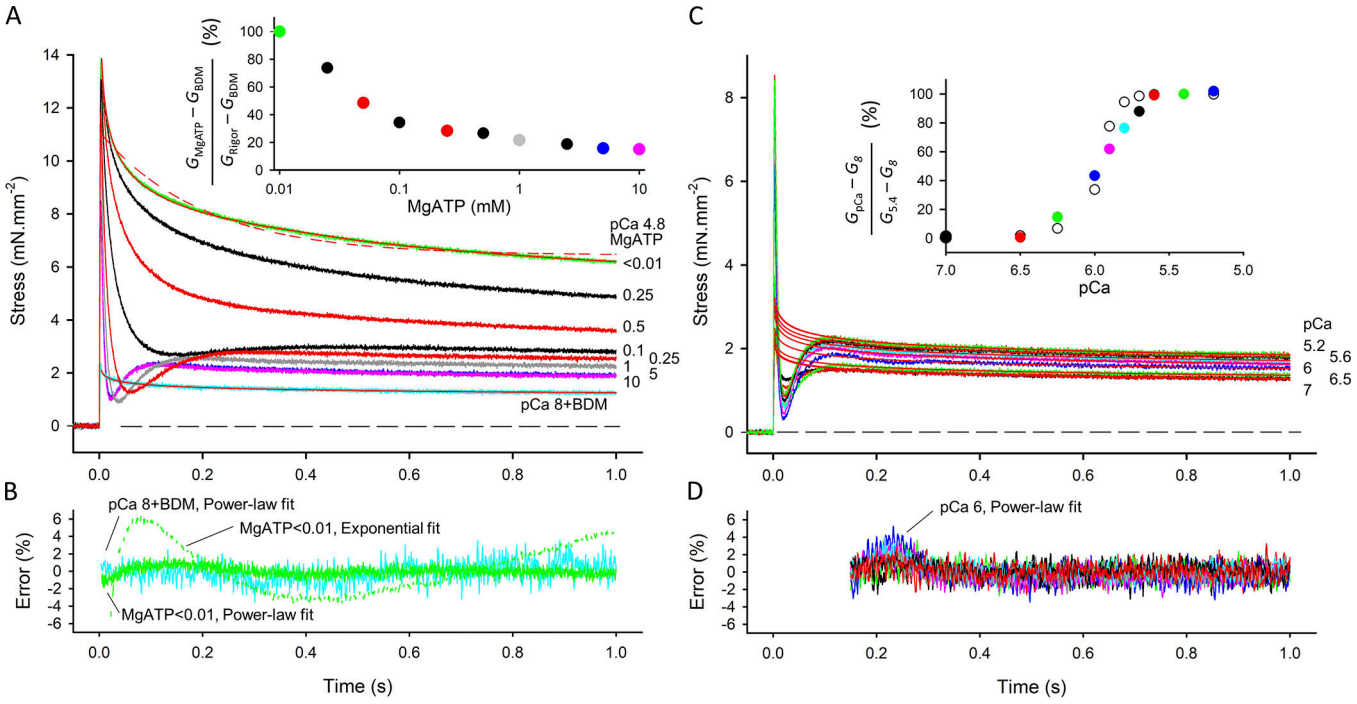

Figure 2. **Force responses to stretch under varying MgATP concentrations in skinned mouse myocardium. (A)** Under maximal Ca^{2+} activation conditions and without MgATP (<0.01 mM, shown in black), the step force response displays the power-law relaxation common for biological tissues (fit in red). The fit to a three-parameter single exponential model appears less appropriate (dashed red). A similar power-law relaxation applies when the muscle is not activated and is bathed in BDM (shown in gray, fit in red). Phases 2 and 3 arise and display faster rates as MgATP is elevated. The stress at t = 1 s corresponds to the amplitude G of the power-law relaxation. If our rationale has merit, the ratio $(G_{MgATP} - G_{BDM})/(G_{Rigor} - G_{BDM})$ should be proportional to the fraction of crossbridges attached and therefore reduced with increasing MgATP, which is known to reduce the myosin crossbridge duty ratio (inset). **(B)** The errors associated with fitting the power-law relaxation to the responses in rigor (green) and relaxed (cyan) were, except for noise, <2%. The error associated with fitting the three-parameter single exponential model to the rigor condition (dotted green) was as high as −30% at 5 ms. **(C)** The power-law also fitted phase 4 at various levels of calcium activation. Full relaxation was observed at pCa 8, maximum activation at pCa 5.4. The ratio $(G_{pCa} - G_8)/(G_{5.4} - G_8)$ displays the sigmoidal relationship with pCa similar to, but not exactly like, that of normalized isometric tension (shown in open circles). **(D)** The fit of the power-law relaxation to the various pCa conditions was within 2% error for most curves and within 4% error for the worst fit. The fits of phase 4 with the power-law relaxation in these datasets suggest that phase 4 reflects a soft glassy viscoelastic response, typical of biological material, with amplitude proportional to myosin crossbridge number.

response (dashed line) was convolved with the four respective kernels to produce four theoretical ramp force responses (solid lines). The measured, actual ramp force responses are overlaid (dotted line). The differences between the theoretical and actual ramp force responses were normalized to the force at 1 s to quantify discrepancies as percentage error. The error between theoretical and actual was consistently <5% throughout the time period examined for all ramps, as illustrated in Fig. 3 F (inset) for 10- and 100-ms ramps. These results demonstrate that the force response of relaxed muscle due to a ramp length change displays the additive property of multiple length perturbations as represented in the convolution kernel.

The additivity test for muscle activated at pCa 5.9 also suggests linearity (Fig. 3 G). The original force response (dashed line) was convolved with the respective kernels to produce the theoretical ramp force responses (solid lines), and the measured force responses are overlaid (dotted line). Errors between theoretical and actual force responses for all four ramp length changes were <10% over the entire time duration recorded and <5% for all but a 10–20-ms portion (Fig. 3 H). Notably, error associated with the 100-ms range was <5% for the entire time period.

The tests of linearity demonstrate that the mechanical properties of both relaxed and activated mouse myocardium under the conditions noted here are reasonably linear to within 5–10% error for length changes of ≤1% ML. For the remainder of this paper, we will assume approximate linearity, which allows us to produce a linear mathematical model and perform further calculations of power and energy required to elongate mouse myocardium.

Modeling force response with strain-dependent myosin crossbridge kinetics

Power-law relaxation

Passive biological tissues often exhibit soft glassy viscoelastic behavior modeled effectively as a power-law stress relaxation in response to an imposed step-length change (Djordjević et al., 2003; Palmer et al., 2013). A power-law relaxation will be used here to describe phase 4 of the step force response. Crossbridge-dependent viscoelasticity represents mechanical contributions of thick filament, myosin S1 and S2, thin filament, and anchoring proteins at the M- and Z-lines (Fig. 4 A). Crossbridge-independent viscoelasticity represents

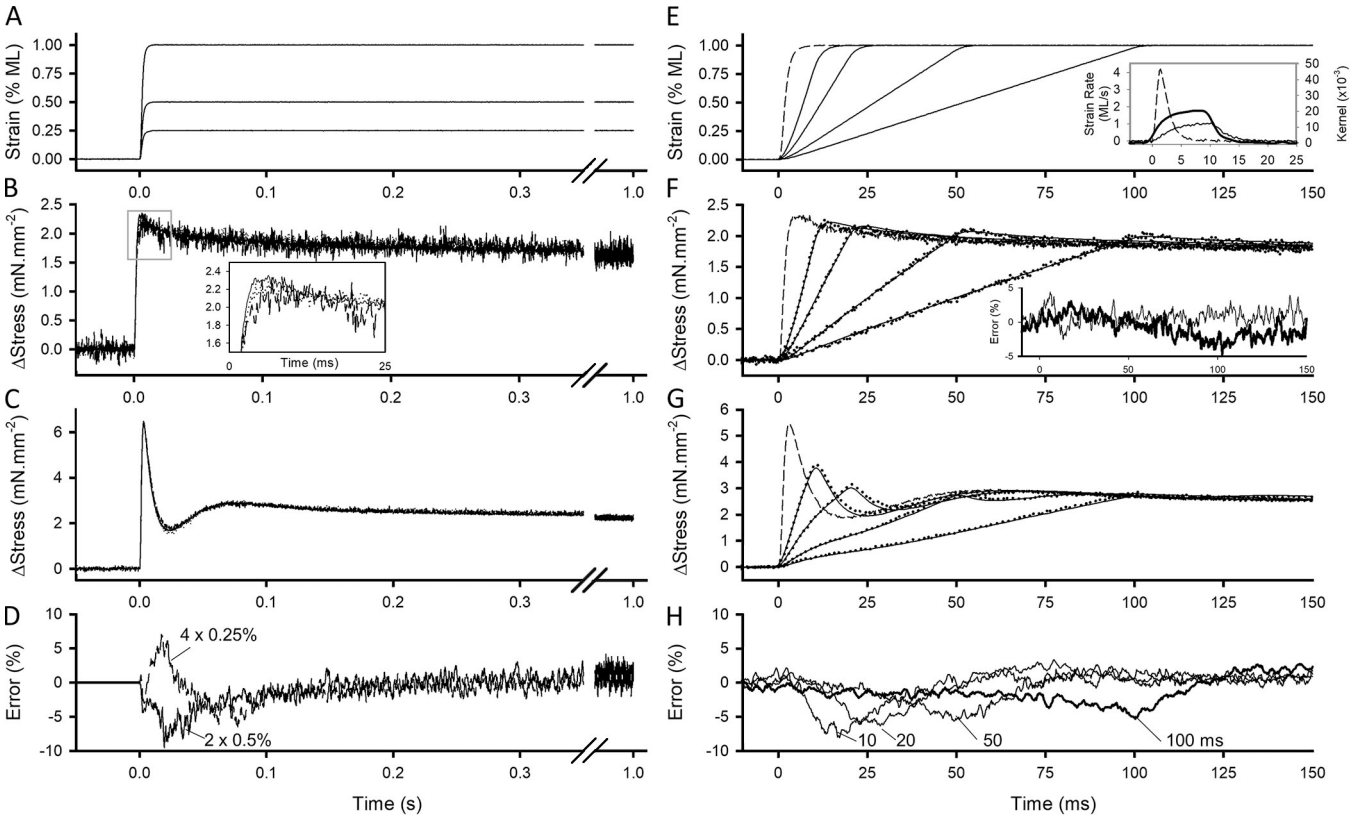

Figure 3. **Linearity of force responses to length changes. (A)** To test homogeneity, three different step-length changes (0.25, 0.5, and 1% ML) were applied to the same preparation of skinned mouse myocardium. **(B)** Under relaxed conditions (pCa 8 + BDM), the respective force responses were multiplied by scaling factors 4, 2, and 1 and superimposed for display. There were no observable differences among the responses except in the first 10 ms (inset). **(C)** At half-maximal Ca^{2+} activation (pCa 5.9), the scaled force responses were again superimposed and are observed to be qualitatively similar. **(D)** Error due to scale was calculated as the difference between scaled responses (0.25 and 0.5% ML) and the 1% ML response normalized to the 1% ML force at 1 s. These errors were as high as 9% but generally no more than 5% error throughout the recorded period. **(E)** To test additivity, a step-length change (dashed line) and four ramp-length changes of varying durations (solid lines) were applied. Each ramp could be generated from the step using a convolution integral, whose kernel was calculated by deconvolving the first derivative of the ramp with that of the step (inset provides example for 10-ms ramp). **(F)** The resulting kernel (bold in inset of E) was then used to calculate theoretical force responses based on the measured step force response. Under relaxed conditions, the theoretical force responses (solid lines) were similar to the measured force responses (dots) that arose when the ramp-length changes were applied. The error between theoretical and measured responses was consistently <5% throughout the recorded period for all ramps. Inset shows examples of 10-ms ramp and 100-ms ramp in bold. **(G)** At half-maximal Ca^{2+} activation, the theoretical ramp force responses (solid lines) were visually similar to the measured ramp force responses (dots). **(H)** Errors were briefly as high as 8% but were generally no more than 5% throughout the recorded period. These demonstrations suggest that the mechanical response of relaxed and activated mouse myocardium to step- and ramp-length changes can be approximated as linear.

the mechanical response of titin, collagen, and any other proteins that can span the half-sarcomere without requiring myosin crossbridge formation (Fig. 4 A). For our purposes here, the crossbridge-dependent and -independent contributions to phase 4 are lumped together as one power-law component that does not explicitly account for any change in myosin kinetics affected by strain. The resting stress due to prestretch and the power-law relaxation after a quick stretch are represented as $\sigma_p(t)$ (Fig. 5 A),

$$\sigma_p(t) = \sigma_{rest} + \varepsilon G_p t^{-k_p} \quad \text{for } t \geq 0, \tag{1}$$

where σ_{rest} = stress before stretch,

$$\varepsilon = \frac{\Delta L}{L_{hs}}$$

length step change in units of strain or fraction of half-sarcomere change, G_p = stiffness modulus in units of mN · mm^{-2}, and k_p = dimensionless constant $0 < k_p < 1$ describing the power-law relaxation. When k_p approaches 0, the sample approaches a purely elastic characteristic; when k_p approaches 1, the sample approaches a purely viscous characteristic.

Strain-dependent crossbridge kinetics

The conceptual model we consider is a two-state model in which the myosin head is in either a strongly bound force-producing state or a weakly bound non–force-producing state. The spatial distribution of newly formed strongly bound crossbridges is given by $f(x)$, which we assume to be symmetrical about $x = 0$, and represents the myosin-binding site on the thin filament relative to a nondisplaced myosin head emanating from the thick filament. The term f_0 = total attachment rate, i.e., integral of $f(x)$ over all x, in units of s^{-1}. We also include an explicit strain dependence on the detachment rate, $g(x) = g_0 + g_1 x$, where g_0 = detachment rate of an unstrained crossbridge in s^{-1} and g_1 =

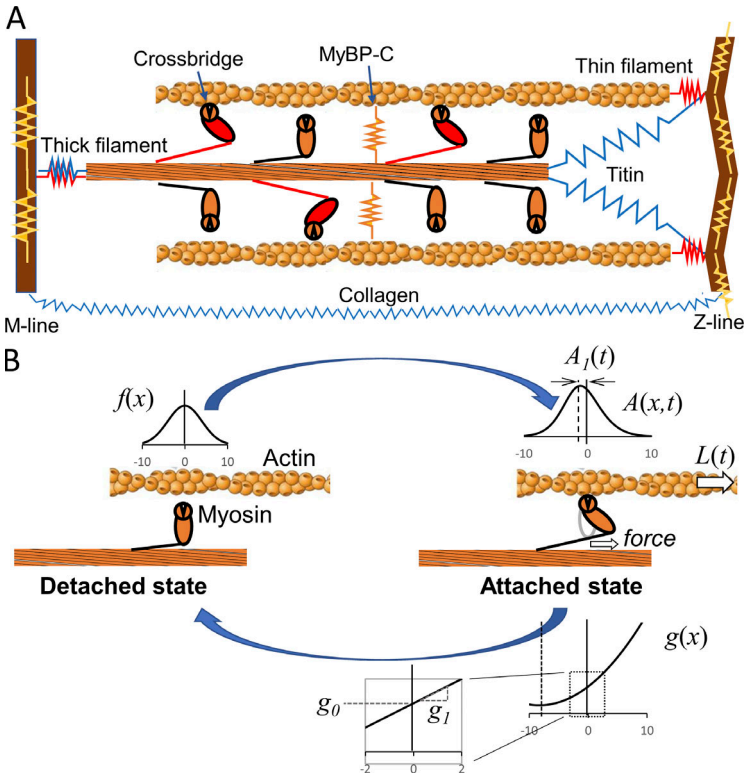

Figure 4. **Cartoon illustration of the half sarcomere and a two-state model of myosin crossbridge formation. (A)** Those protein connections that span the half sarcomere and are responsible for crossbridge-independent viscoelasticity include most notably titin and collagen (blue). Protein connections responsible for crossbridge-dependent viscoelasticity include myosin and other proteins of the thick and thin filaments and the M- and Z-lines such as actin, α-actinin, etc. (red). Still other proteins, such as myosin-binding protein C, contribute to a transverse stiffness that can play indirect roles in longitudinal viscoelasticity (orange and yellow). **(B)** The two-state model developed here assumes a non–force-producing detached state and a force-producing attached state. The rate of transition from detached to attached is a function of x, $f(x)$, that signifies the spatial distribution of newly formed crossbridges. This distribution is modeled as Gaussian and, importantly, evenly symmetric about a central point we define as $x = 0$. Crossbridges in the attached state are spatially distributed according to $A(x,t)$, with a mean displacement that is not symmetric about $x = 0$ owing to the strain dependence of the detachment rate, $g(x)$. In this example, detachment rate is modeled to be enhanced with positive strain, i.e., stretch, and reduced with negative strain, i.e., compression, as signified by the proportionality constant g_1. Under no strain, the detachment rate is a constant g_0.

sensitivity of detachment rate to crossbridge displacement in $s^{-1} \cdot nm^{-1}$ (Fig. 4 B). The positive sign associated with g_1 signifies that detachment rate $g(x)$ is enhanced with muscle lengthening. The Supplemental text (see bottom of PDF) presents a full derivation of the mathematical model. The key results are presented here.

The mean displacement of the attached crossbridges, $A_1(t)$, was derived as follows:

$$A_1(t) = \bar{A}_1 + \Delta L \bar{A}_0 e^{-g_0 t} \text{ for } t \geq 0, \quad (2)$$

where $\bar{A}_1$ = the mean displacement of crossbridges under isometric conditions in units of nm, and $e^{-g_0 t}$ = exponential function with a decay rate equal to crossbridge detachment rate g_0 s^{-1}. In practice, ΔL is ≤1% of the resting half-sarcomere length, i.e., ≤10 nm for a half sarcomere of ∼1 µm, to best ensure a linear response. An example $A_1(t)$ for 10-nm stretch is shown in Fig. 5 B. The expected force due to displacement of myosin crossbridges requires the multiplication of Eq. 2 by N_{hs}, the total number of available myosin crossbridges in a half-sarcomere, and k_{stiff}, the stiffness of each crossbridge in units $pN \cdot nm^{-1}$. The associated stress, $\sigma_1(t)$, is calculated by normalizing to *CSA*:

$$\sigma_1(t) = \lambda \bar{A}_1 + \varepsilon L_{hs} \lambda \bar{A}_0 e^{-g_0 t} \quad \text{for } t \geq 0, \quad (3)$$

where

$$\lambda = \frac{N_{hs} k_{stiff}}{CSA}$$

with units $pN \cdot mm^{-2} \cdot nm^{-1}$, and the product $L_{hs}\lambda$ represents the mean elastic modulus of any available crossbridge in units $pN \cdot mm^{-2}$. An example $\sigma_1(t)$ is provided in Fig. 5 B.

The mean crossbridge displacement defined above in Eq. 2 can be used to derive the effects of strain on detachment rate and the total number of myosin crossbridges attached. For a small perturbation ensuring a linear response, the fraction of myosin heads attached in response to a small step-length change of ΔL would have the following form:

$$A_0(t) = \bar{A}_0 - \Delta L \frac{g_1 \bar{A}_0}{f_0} \left(e^{-g_0 t} - e^{-(f_0 + g_0)t} \right) \quad \text{for } t \geq 0. \quad (4)$$

Eq. 4 describes a transient reduction in the fraction of force-producing myosin crossbridges attached after a step-length change (Fig. 5 C). The g_0-exponential term describes the new equilibration point for the fraction of crossbridges attached due to strain imposed on them, and the $(f_0 + g_0)$-exponential term represents the rate of reequilibration in a two-state model (Brenner, 1988). The force attributable to this fraction of myosin crossbridges would require the multiplication of N_{hs}, the total number of available myosin crossbridges in a half-sarcomere, and F_{uni}, the unitary force produced by each myosin crossbridge in units of pN. The stress due to the fraction of myosin crossbridge attached, $\sigma_0(t)$, requires normalizing to *CSA*:

$$\sigma_0(t) = \gamma \bar{A}_0 - \varepsilon L_{hs} \gamma \frac{g_1 \bar{A}_0}{f_0} \left(e^{-g_0 t} - e^{-(f_0 + g_0)t} \right) \quad \text{for } t \geq 0, \quad (5)$$

where

$$\gamma = \frac{N_{hs} F_{uni}}{CSA}$$

with units $pN \cdot mm^{-2}$ and represents the active stress generated by myosin crossbridges in the half-sarcomere. An example $\sigma_0(t)$ is also shown in Fig. 5 C.

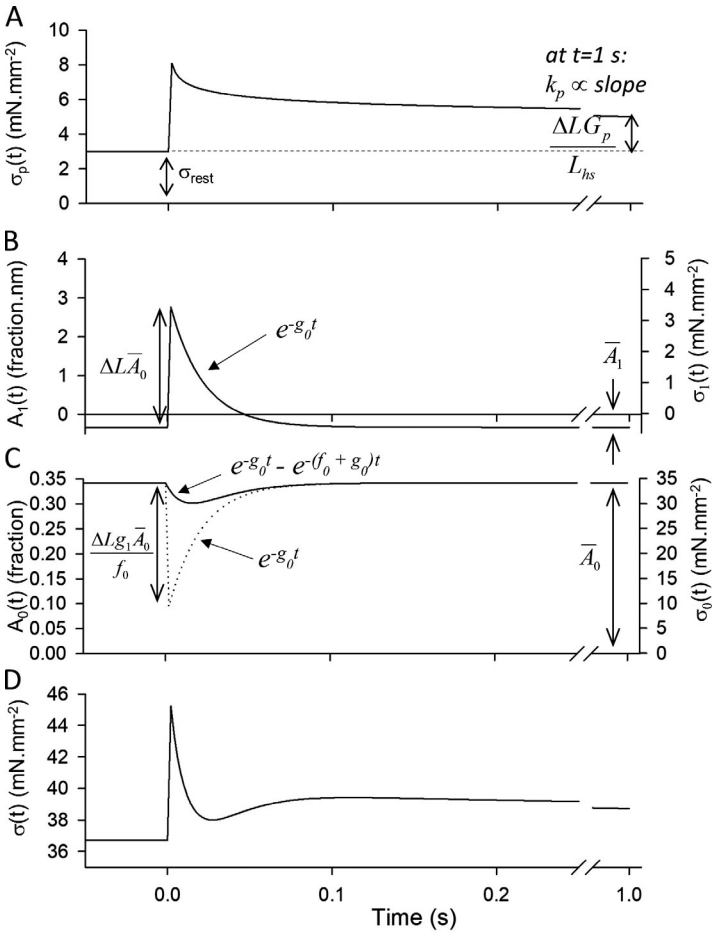

Figure 5. **Example components of our model describing the step force response of activated muscle to a quick stretch. (A)** A power-law relaxation after a quick stretch, $\sigma_p(t)$, is used to represent phase 4. **(B)** The mean crossbridge displacement $A_1(t)$ is a negative value until the step, which imposes a positive-going mean displacement. The positive displacement is then relaxed with a rate constant of g_0. The stress due to the displacement of crossbridges, $\sigma_1(t)$, is on the order of mN · mm^{-2} in this example. **(C)** The positive mean displacement shown in B leads to a higher probability of crossbridge detachment according to $g(x)$ resulting in a transiently reduced equilibrium point (dotted line) and transient reduction in the fraction of crossbridges attached, $A_0(t)$, attempting to reach equilibrium. The stress attributable to the fraction of crossbridges formed, $\sigma_0(t)$, is on the order of tens of mN · mm^{-2} in this example. **(D)** All components together generate a step force response similar in shape to that recorded with a muscle sample. Parameters used to generate this figure were f_0 = 25 s^{-1}, SD of $f(x)$ distribution = 5 nm, f_2 = 625 s^{-1} · nm^2, g_0 = 50 s^{-1}, g_1 = 2 s^{-1} · nm^{-1}, N = 10^{13} available myosin, CSA = 1 mm^2, k_{stiff} = 0.15 pN · nm^{-1}, ΔL = 10 nm, L_{hs} = 1,000 nm, F_{uni} = 10 pN, σ_{rest} = 3 mN · mm^{-2}, G_p = 20 mN · mm^{-2}, and k_p = 0.15 (unitless).

Full step response

The full step stress response based on the above model is given as follows (Fig. 5 D):

$$\sigma(t) = \sigma_{rest} + \varepsilon G_p t^{-k_p} + \gamma \bar{A}_0 - \varepsilon L_{hs} \gamma \frac{g_1 \bar{A}_0}{f_0} \left(e^{-g_0 t} - e^{-(f_0+g_0)t}\right) + \lambda \bar{A}_1 + \varepsilon L_{hs} \lambda \bar{A}_0 e^{-g_0 t}. \quad (6)$$

For the remainder of this paper, we focus on the viscoelastic response, i.e., the change in stress, Δσ, due to a quickly imposed strain of ε:

$$\Delta\sigma(t) = \varepsilon G_p t^{-k_p} - \varepsilon L_{hs} \gamma \frac{g_1 \bar{A}_0}{f_0} \left(e^{-g_0 t} - e^{-(f_0+g_0)t}\right) + \varepsilon L_{hs} \lambda \bar{A}_0 e^{-g_0 t}. \quad (7)$$

Fitting the model to recorded data

Using the analytical solution provided in Eq. 7, we estimated the model parameters that generated the best fits to step force responses collected in skinned mouse myocardial strips activated at pCa 5.9 and exposed to increasing Pi. We observed that isometric stress before stretch was correspondingly reduced from 18.1 to 16.4 mN · mm^2 as Pi was raised from 1 to 8 mM (Smith and Geeves, 1995; Ranatunga, 1999). For our purposes, the isometric stress was subtracted from recorded stress, and the change in stress, Δσ, was examined as a reflection of myocardial viscoelasticity. Fig. 6 A illustrates the force responses recorded for 1, 3, and 8 mM Pi. For almost all muscles examined, the magnitude of phase 4 was reduced with increasing Pi. However, we focused on this dataset specifically because of the similarities in phase 4 among the different Pi conditions. The consequences of Pi on myosin crossbridge kinetics are then readily observed in phases 2 and 3. The fits of Eq. 7 to Δσ are superimposed on the recorded data, and parameter estimates are given in Table 1. We then assessed the results of the fits and the reasonableness of the model parameters.

Power-law relaxation

The power-law relaxation component of the force response, $\Delta\sigma_p$, did not appreciably differ among the three Pi concentrations as selected and therefore are indistinguishable in Fig. 6 B. The modulus G_p and viscous-elastic ratio k_p that describe the power-law relaxation characteristic were not found to be dependent on Pi in these examples (correlation coefficients = 0.527 and −0.587, respectively, were not statistically significant; Table 1).

Mean displacement of attached crossbridges

The mean displacement of crossbridges due to stretch results in the stress $\Delta\sigma_1$ (Fig. 6 C). This component of the force response corresponds to the elastic force generated from the initial stretch of crossbridges and the exponential decay of that force as these crossbridges detach. The interpretation of this component of the force response appearing in several previous models would seem intuitively appropriate (Kawai and Brandt. 1980; Palmer et al., 2007).

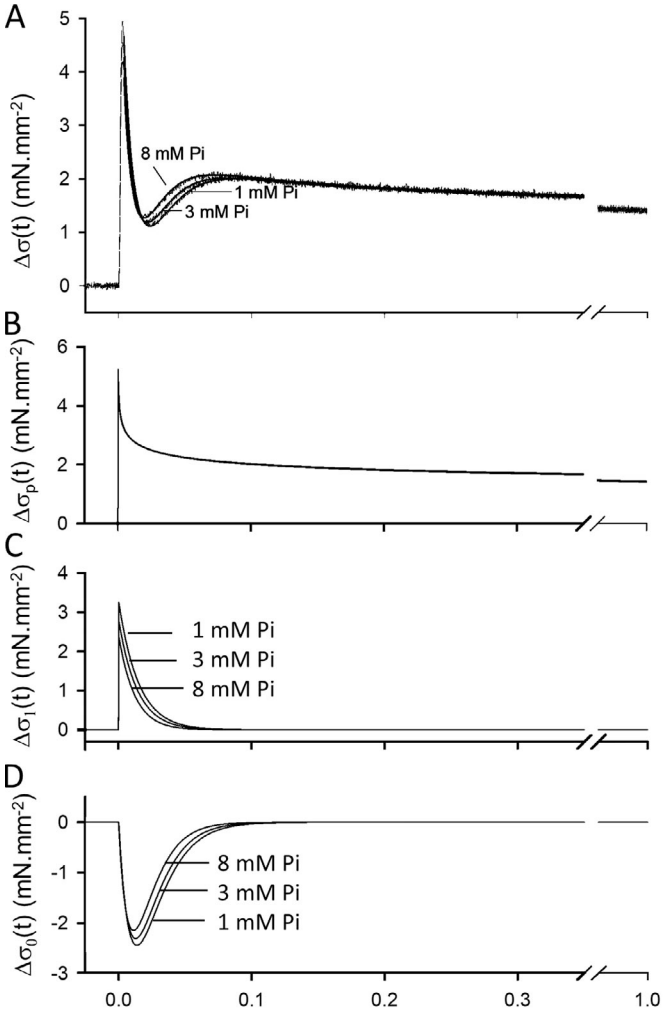

Figure 6. **Results of fits of the model to recorded step force responses.** **(A)** With varying Pi, the analytical model (solid lines) fits the step force responses well. **(B)** The power-law relaxation component appears little affected by varying Pi in these examples. **(C)** According to model fits, the mean displacement of crossbridges and corresponding stress ($\Delta\sigma_1$) was reduced in magnitude and quicker to relax with higher Pi, which is expected. **(D)** The fraction of crossbridges attached and corresponding stress shown ($\Delta\sigma_0$) demonstrated a reduced nadir with higher Pi. This finding would suggest that the higher Pi led to higher rate constants in such a way as to reduce the force drop between phases 2 and 3.

The decay rate shown in Fig. 6 C, which corresponds to g_0, is enhanced with higher Pi (supported by a correlation coefficient = 0.990 in Table 1), which would be expected if Pi facilitates detachment before MgADP release. It is noteworthy that the amplitude of $\Delta\sigma_1$, directly proportional to parameter $L_{hs}\lambda\bar{A}_0$, is reduced with increasing Pi (correlation coefficient = −0.808 in Table 1), which is consistent with Pi enhancing the detachment rate under steady-state conditions. So far, we would infer that our modeling of mean displacement of attached crossbridges corresponds to the expected effects of Pi.

Fraction of crossbridges attached

The transient reduction in crossbridge-generated stress is presented as $\Delta\sigma_0$ in Fig. 6 D. The nadir in the fraction of attached crossbridges is shallower with higher Pi, primarily because the rate of force redevelopment phase (corresponding to phase 3) was faster with higher Pi. The attachment rate f_0 is reduced with higher Pi (correlation coefficient = −0.862 in Table 1), as would be expected from Pi inhibiting crossbridge formation and the generation of a power stroke. The sensitivity of the myosin crossbridge detachment rate to stretch was represented within the parameter

$$\left(L_{hs}\gamma\frac{g_1\bar{A}_0}{f_0}\right)$$

and was enhanced with higher Pi (correlation coefficient = 0.842). These results with varying Pi are consistent with the idea that Pi facilitates detachment with sarcomere lengthening, which is equivalent to resistive load placed on the myosin crossbridge before MgADP release.

Stress, power, and energy required to elongate myocardium

To demonstrate that the stretch-enhanced detachment of myosin results in reduced resistance to myocardial lengthening, we modeled the length change experienced by ventricular myocardium during diastole as a 1% ML change over 100 ms (Fig. 7 A). We then generated the total stress response, $\Delta\sigma$, for 1, 3, and 8 mM Pi (Fig. 7 B) from the respective step force responses convolved with the 100-ms kernel described earlier in Fig. 3 E. The stress changes shown in Fig. 7 B represent the muscle responses to a constant length change over 100 ms. The hypothetical power-law response displayed in Fig. 7 B corresponds to the power-law relaxation calculated for phase 4 in Fig. 6 B that would arise if there were no transient reduction in force, i.e., if there were no phases 2 and 3. The comparison with the hypothetical power-law response demonstrates that the transient depression in force, as we hypothesize occurs with an enhanced detachment rate during lengthening, would result in a lower stress required to achieve the ramp lengthening profile over 100 ms.

Mechanical power is defined as the product of the stress and strain rate. The mechanical power per volume of muscle sample that must be applied to the muscle to achieve the 1% length change can therefore be easily calculated from stress and strain rate (Fig. 7 C). The mechanical energy per sample volume is then calculated as the time integral of the power (Fig. 7 D). The inset of Fig. 7 D illustrates that the energy required to perform the 100-ms stretch was lower at 3 mM Pi compared with 1 mM, but higher at 8 mM. This result demonstrates that the energy expenditure for a stretch depends on many factors that make up the muscle viscoelasticity, including myosin kinetics, stretch speed, and stretch duration. In short, faster myosin kinetics do not necessarily lead to less energy expenditure.

It should be noted that these calculations of stress, power, and energy are not based on our model. Only the hypothetical power-law responses shown throughout Fig. 7 result from the power-law model of phase 4. In all these examples, the stress, power, and energy required to elongate the muscle 1% ML over 100 ms are lower than that required from the hypothetical power-law response.

Computer simulation of stretch

We used a computer model to estimate the effects of a length change on the number of myosin crossbridges attached or

Table 1. **Parameter estimates resulting from fitting Eq. 7 to step force responses recorded in skinned mouse myocardium exposed to varying Pi at approximately half Ca^{2+} activation, pCa 5.9**

Condition	G_p (mN · mm^{-2})	k_p	$\left(L_{hs}\gamma\frac{g_1\bar{A}_0}{f_0}\right)$ (mN · mm^{-2})	$(L_{hs}\lambda\bar{A}_0)$ (mN · mm^{-2})	$f_0 + g_0$ (s^{-1})	g_0 (s^{-1})	f_0 (s^{-1})
[Pi] (mM)							
1.0	142	0.154	37.2	3.25	80.6	67.2	13.4
2.0	139	0.159	35.4	2.91	84.3	70.1	14.2
3.0	141	0.154	34.2	2.78	86.4	71.9	14.5
4.0	143	0.149	36.6	2.53	89.3	75.9	13.4
5.0	139	0.157	38.2	2.21	90.3	77.7	12.6
8.0	144	0.148	49.2	2.43	93.6	83.1	10.5
r	0.527	−0.587	**0.842**	**−0.808**	**0.962**	**0.990**	**−0.862**
P	0.283	0.288	**0.036**	**0.049**	**0.002**	**<0.001**	**0.027**

The correlation coefficient, *r*, refers to the Pearson coefficient between the given parameter and Pi condition; *r* values shown in bold demonstrate statistical significance at P < 0.05.

detached over the course of a prolonged stretch. Both early and late filling periods last ∼100 ms in healthy adults and stretch the circumference of the ventricle on the order of an additional 1–20% (Zhang et al., 2019). In our experience, the characteristic time points of a force response due to α-myosin kinetics in mouse myocardium at 17°C are roughly those of β-myosin kinetics in human myocardium at 37°C (unpublished data). Therefore, for illustrative purposes, we modeled the effects of a 1% stretch over 100 ms using parameters suggested from the fit of the model to the data recorded from mouse myocardium under the 17°C and 1-mM Pi conditions (Fig. 8 A).

A computer simulation of the fraction of myosin heads attached and detached showed that the fraction of myosin heads in the attached state is reduced with imposed constant strain rate on the muscle and reaches a lower steady-state value within ∼50 ms (Fig. 8 B). This lower number of crossbridges during a steady lengthening was predicted previously by Smith and Geeves (1995). Conversely, the fraction of detached myosin heads is elevated with the same magnitude and dynamics. These changes in the fractions of heads attached and detached result from the enhanced detachment rate of the myosin crossbridges as they experience increasingly greater strain during the simulated stretch.

After applying the necessary constants to express stress as would be recorded from a muscle, we simulated the stress response and its components (Fig. 8 C). The stress $\sigma_1(t)$ due to the mean displacement $A_1(t)$ is small and negative valued before stretch, because there is a bias for longer-lived crossbridges with negative strain. The values of $\sigma_1(t)$ and $A_1(t)$ then become positive at a maximum of ∼0.5 mN · mm^{-2} during the imposed constant strain rate. This stress corresponds to the elastic recoil force that arises from the stretching of attached myosin crossbridges. The stress $\sigma_0(t)$ due to the fraction of crossbridges attached $A_0(t)$ and generating F_{uni} is reduced as the number of attached crossbridges is reduced during the period of imposed constant strain rate. This reduction in the number of force-generating crossbridges illustrates that an enhanced detachment rate due to strain on the crossbridge could account for a transient loss of crossbridge number. The stress $\sigma_p(t)$ due to the power-law relaxation of the muscle reflects the expected power-law stress relaxation that would be expected to occur if there were no change in detachment rate with strain (Fig. 8 C). A hypothetical power-law response, which reflects the response expected if there were no change in detachment rate with strain (dotted line in Fig. 8 D), i.e., $\sigma_{rest} + \sigma_p(t)$, is also shown for comparison purposes.

The total stress response, i.e., the sum $\sigma_1(t) + \sigma_0(t) + \sigma_p(t)$, that resulted from the computer model is qualitatively similar in dynamics to that recorded from real mouse myocardium (Fig. 3 G). When compared with the hypothetical power-law response, it is clear that the stretch of the muscle is accomplished with less stress when an enhanced detachment rate due to strain is available. Consequently, the total energy required to stretch the myocardium 1% over 100 ms (Fig. 8 D) would also be reduced when the myosin detachment rate is enhanced with strain.

Discussion

Our study demonstrates that a strain-dependent enhancement of myosin crossbridge detachment sufficiently explains the step force response observed in cardiac muscle after a quick stretch. It should be noted that we have not proven this to be the case, only that it is plausible. Our findings suggest that phases 2 and 3 of the typical step force response could arise from a transiently reduced myofilament force due to a briefly enhanced crossbridge detachment rate caused by strain on those crossbridges already attached when stretch occurs followed by their reattachment. We further suggest that the elevated force of phase 4 does not reflect a stretch activation of the thin filament, but rather the tail of a power-law viscoelastic response commonly found in biological tissues. Our interpretation differs significantly from conventional interpretations of these data and, therefore, could offer novel insights into the physiological mechanisms that underlie diastolic function in mammalian cardiac muscle.

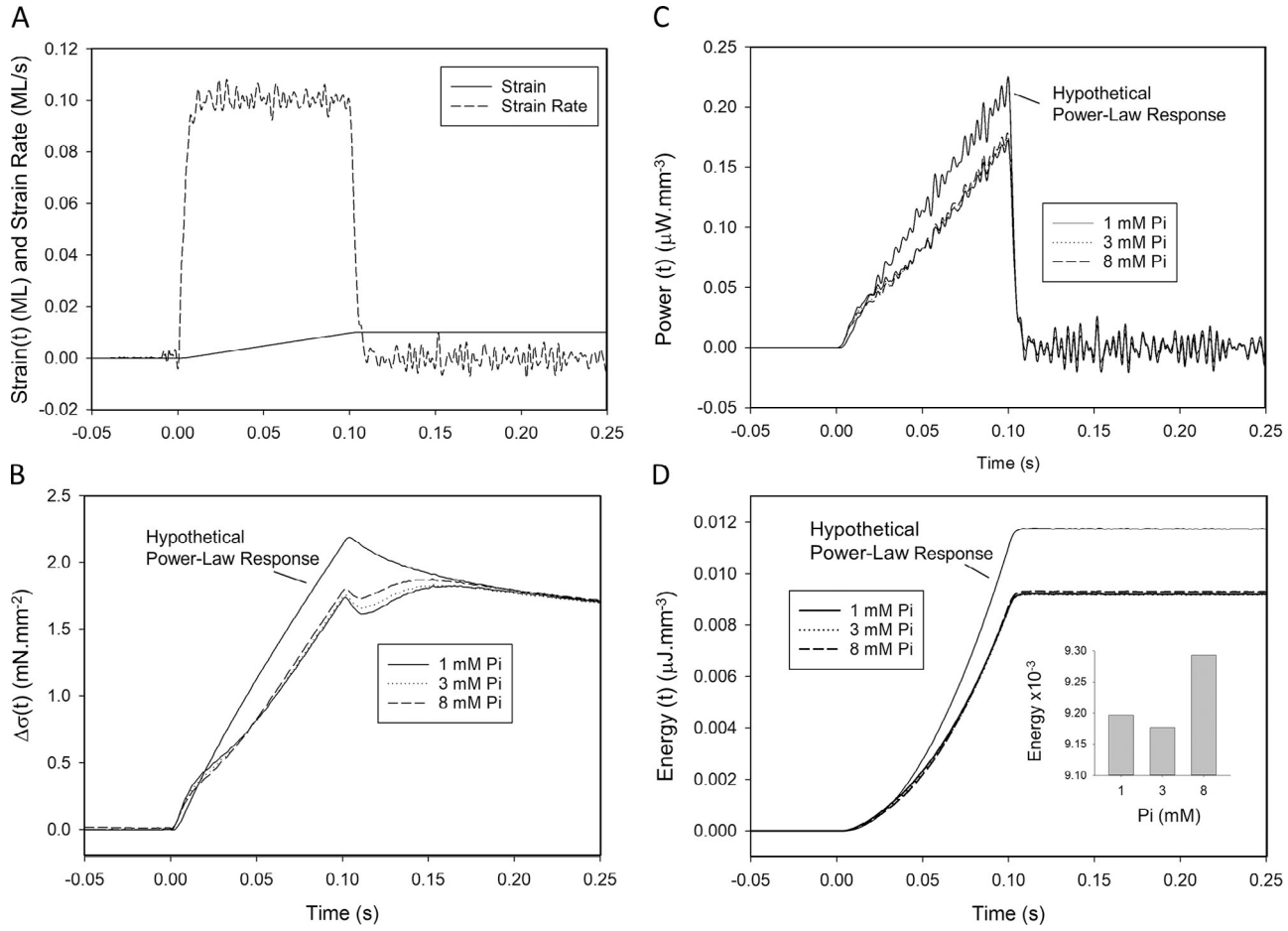

Figure 7. **Stress, power, and energy required to stretch 1% ML over 100 ms, which mimics late diastolic filling. (A)** A strain of 1% ML is applied over 100 ms. The strain rate is ∼0.1 ML/s over the same 100 ms. **(B)** The stress required to stretch the muscle 1% over 100 ms, reflected in $\Delta\sigma(t)$, is compared against the hypothetical power-law response extrapolated from the fit to phase 4. With myosin detachment enhanced by stretch, the stress required to stretch the muscle is reduced compared with the hypothetical power-law response. **(C)** The mechanical power per muscle volume required to stretch the muscle 1% over 100 ms was calculated as the product of stress and strain rate. The power required to stretch the muscle was reduced compared with the hypothetical power-law response. **(D)** The mechanical energy per muscle volume required to stretch the muscle 1% over 100 ms is lowered by ∼25% compared with the hypothetical power-law response. The total energy required to perform this stretch is lower for 3 mM Pi compared with 1 mM but is highest for 8 mM (inset). This comparison demonstrates that faster myosin kinetics do not necessary lead to more favorable energy expenditure.

The prevailing interpretation of the force response to a quick stretch has centered on the enhanced activation of the thin filament regulatory proteins, troponins and tropomyosin, due to the strain experienced during and after a stretch (Campbell, 1997; Moss et al., 2004; Campbell and Chandra, 2006; Stelzer and Moss, 2006). This enhanced activation of the thin filament due to stretch may play some role in cardiac muscle as it does in insect flight muscle, where the activating and deactivating movements of troponins and tropomyosin can be elicited by a 2% stretch (Perz-Edwards et al., 2011). However, thin-filament regulatory proteins are not required to induce the typical step force response in mammalian cardiac muscle. In a series of studies by Kawai and colleagues, bovine cardiac muscle lacking thin-filament regulatory proteins still displayed the characteristic features expected of a typical step force response. Specifically, after thin filaments were removed and actin filaments were reconstituted without regulatory proteins, the complex modulus detected using sinusoidal analysis displayed (a) the prominent peak in the viscous modulus at high frequencies, corresponding to phase 2, (b) the prominent negative viscous modulus at low frequencies, corresponding to phase 3, and (c) positive-valued elastic and viscous moduli at the lowest frequency, corresponding to phase 4 (Fujita and Kawai, 2002; Fujita et al., 2002; Lu et al., 2005; Kawai and Ishiwata, 2006). Thus, an effect of stretch on the thin filament is not necessary to invoke as the primary underlying mechanism of the force response to stretch. We hypothesized instead that the typical force response to a quick stretch is due to the enhanced detachment rate in those crossbridges that were under strain.

Using a two-state model, we have not assigned or assumed where in the crossbridge cycle a strain due to stretch could influence myosin detachment rate. It is reported that the rate of MgADP release in cardiac myosin and in smooth muscle myosin, another class II myosin like cardiac myosin, is slowed by a resistive load, which corresponds to muscle stretch (Veigel et al., 2005; Kad et al., 2007; Liu et al., 2018). In the context of those

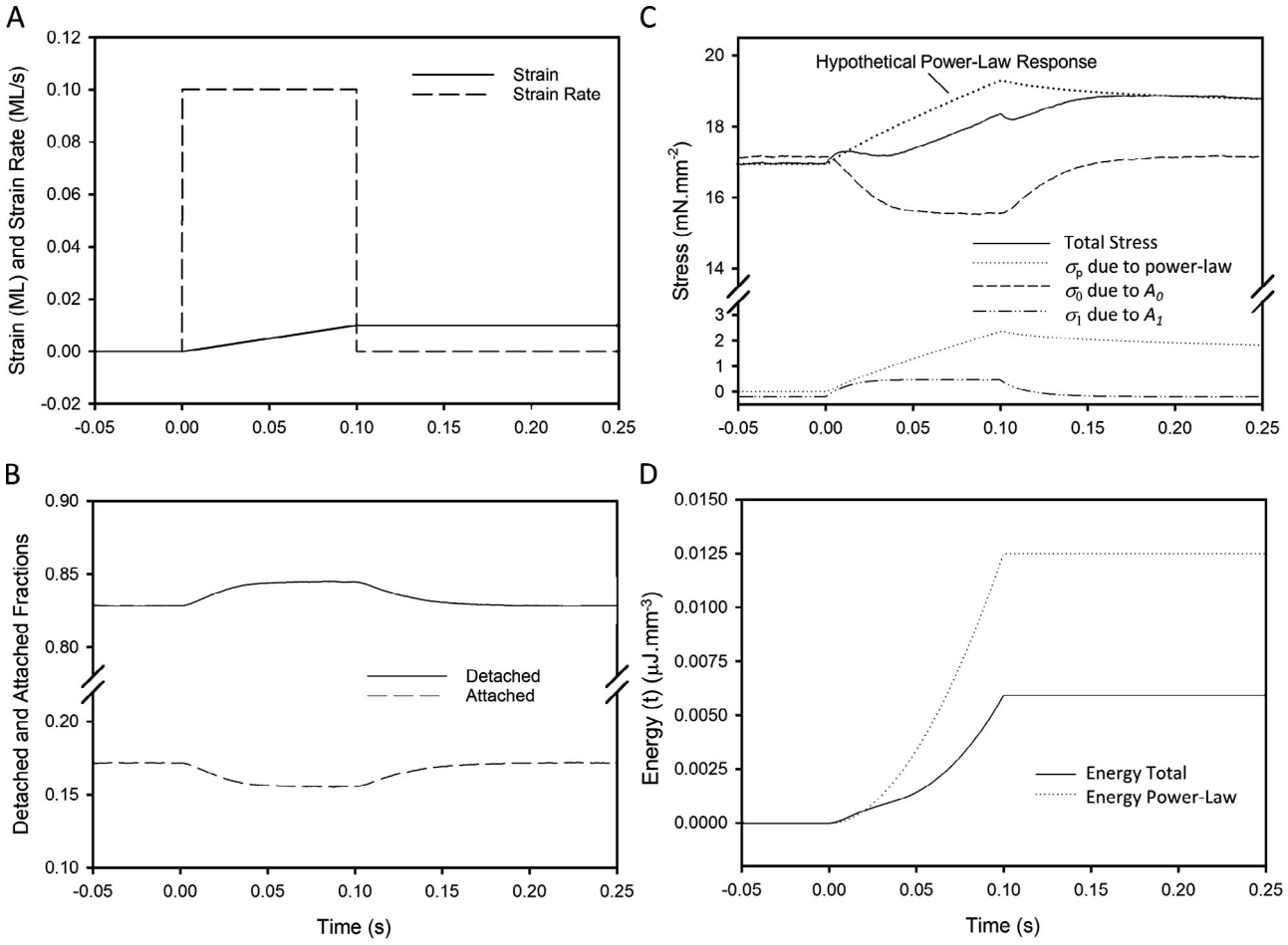

Figure 8. **Results of computer simulation of muscle force response to a 1% stretch over 100 ms. (A)** The strain in this case is a perfect ramp to 1% strain over 100 ms. The strain rate is a constant 0.1 ML/s over that period. **(B)** The states, either attached or detached, of 5 million myosin heads were simulated using rate constants estimated from the case of 1 mM Pi in real muscle (Fig. 5 B and Table 1). **(C)** The enhanced detachment rate with strain on the crossbridge resulted in a reduced fraction of force-producing crossbridges attached and an enhanced fraction of detached during and immediately after the stretch. This result suggests that an enhanced crossbridge detachment rate with stretch can explain the enhanced relaxation during stretch (Chung et al., 2017). **(D)** An enhanced detachment rate with stretch would permit stretch with less mechanical energy compared with the hypothetical power-law response. Parameters used in this simulation were f_0 = 13.4 s^{-1}, SD of $f(x)$ = 2 nm, f_2 = 53.6 $s^{-1} \cdot nm^2$, g_0 = 67.2 s^{-1}, g_1 = 6 $s^{-1} \cdot nm^{-1}$, N = 10^{10} available myosin per half sarcomere · mm^{-2}, CSA = 1 mm^2, k_{stiff} = 0.3 pN · nm^{-1}, ΔL = 10 nm, L_{hs} = 1,000 nm, F_{uni} = 10 pN, σ_{rest} = 0 mN · mm^{-2}, G_p = 142 mN · mm^{-2}, and k_p = 0.154 (unitless).

findings, our results would suggest that enhanced detachment with stretch must occur before MgADP release. Such a strain-dependent detachment could involve reversal of the myosin power stroke, which has been observed and modeled to be sensitive to Pi availability (Dantzig et al., 1992; Smith and Geeves, 1995), or possibly without reversal but still sensitive to Pi (Debold et al., 2013). Other observations consistent with either mechanism include a Pi-enhanced rate of tension development after rapid temperature change (Ranatunga, 1999), a significantly shorter myosin crossbridge lifetime observed in the laser trap assay when Pi is abundant (Baker et al., 2002), a reduced rate of free Pi generation in activated striated muscle undergoing stretch (Mansfield et al., 2012), and an enhanced oscillatory work and power with increasing Pi (Zhao and Swank, 2013).

Our own observations with increasing Pi concentration are consistent with the idea that Pi acts to enhance crossbridge detachment rate, i.e., g_0 in our model, as noted by a positive correlation between g_0 and Pi in Table 1. Because g_0 also incorporates detachment due to MgATP binding in our two-state model, we surmise that the two-state model, while useful in the present demonstration, is not adequate to describe the full interplay between biochemical and mechanical influences on myosin crossbridge kinetics. We would need at least two force-producing states in future modeling efforts relevant to conditions with saturating MgATP. With at least two force-producing states, the rate of reversal could be made explicitly dependent on Pi availability and the strain imposed on the crossbridge during lengthening, as proposed previously (Dantzig et al., 1992; Smith and Geeves, 1995; Ranatunga, 1999; Houdusse and Sweeney, 2001; Zhao and Swank, 2013). Such a mechanism would have significant implications for our understanding of striated muscle relaxation function, including cardiac diastole.

Relevance to diastolic function

Ventricular diastole can be considered to occur in four phases: isovolumic relaxation, early filling, diastasis (when little filling

occurs), and late filling. Isovolumic relaxation commences when the aortic valve closes as myocardial contractile force subsides with diminishing intracellular Ca^{2+} activation of contractile force. During this phase, the ventricular myocardium, which had been compressed during systole, begins to rebound due to stored elastic energy. The latter causes shape changes during this phase, but overall relengthening cannot begin until the mitral valve opens. This occurs when the LV pressure falls below the left atrium (LA) pressure, and early filling ensues. During early filling, the ventricular myocardium undergoes overall relengthening driven by the stored elastic energy, which produces a suction that draws blood into the enlarging LV from the LA, as well as by the level of LA pressure at the time of mitral valve opening (Bell et al., 2000). Early filling is not considered an energy-consuming process and accounts for as much as ∼80% of the end-diastolic volume of the normal human adult LV (Zhang et al., 2019). Once LV and LA pressures equilibrate, early filling ceases and a diastatic phase commences with little or no filling. The length of this phase is variable and largely dependent on heart rate. Late filling then occurs when the LA actively pumps blood into the LV immediately before ventricular systole. In a normal human adult LV, the endocardium may lengthen an additional 4–6% and the epicardium 1–3% over a span of ∼100 ms during late filling (Zhang et al., 2019). This seemingly small percentage change in myocardial length represents as much as ∼20% increase in chamber volume and plays an important part in normal LV filling.

If the LV myofilaments produce contractile force at any time during diastole, due to the normal basal level of Ca^{2+}-independent activation of the thin filament observed in human myocardium (Donaldson et al., 2012) or due to incomplete removal of intracellular Ca^{2+} as observed in normal and more so in hypertrophied human LV (Selby et al., 2011; Runte et al., 2017), the myocardium will resist lengthening, and end-diastolic chamber volume may not reach its fullest extent before systole begins. In this way, a persistent contractile force produced by myosin crossbridges contributes to the viscoelastic stiffness of ventricular myocardium throughout diastole and thereby plays a significant role in diastolic dysfunction.

With an important set of observations, Chung et al. (2017) reported that lengthening the myocardium at the end of systole enhanced relaxation in proportion to the rate of relengthening. These findings mirror those reported in a whole heart, which experienced faster relaxation when load on the LV was artificially enhanced in late systole (Zile and Gaasch, 1991). Those observations, like ours, were made at the macroscopic level, where relengthening in diastole takes place with a strain rate over time periods lasting up to 100 ms. The myosin crossbridge is relatively short-lived, on the order of 10–40 ms on average (Tyska and Warshaw, 2002). Therefore, an attached myosin crossbridge would experience significant strain during diastolic relengthening and would be subjected to any strain dependence on its kinetics.

The mitigation of crossbridge force during increasing myocardial strain rate due to the underlying myosin crossbridge strain may be an important contributor to filling function in all phases of diastole, because some level of thin filament activation persists throughout diastole. A measurable myofilament force is produced in human myocardium at normal and elevated diastolic Ca^{2+} (Selby et al., 2011; Runte et al., 2017) and at non-activating Ca^{2+} concentrations (Gong et al., 2005; Donaldson et al., 2012). Strongly bound myosin crossbridges can also contribute to thin filament activation due to elevated MgADP, which can accompany and compound heart failure (Sequeira et al., 2015). Therefore, either with or without compromised calcium ion handling, some level of contractile force is present throughout diastole (Moss et al., 2004) and would contribute to myocardial stiffness and oppose LV myocardial lengthening and chamber filling. The findings of Chung et al. (2017) and Zile and Gaasch (1991) would therefore be applicable throughout diastole, including late diastole. A reversal of the myosin power stroke, as we have proposed here in response to a positive strain (or resistive load) on the crossbridge, would reduce myocardial stiffness and ease ventricular filling as well as reduce unnecessary utilization of MgATP. The reversal of the power stroke during stretch would ensure, or at least bias, that the energy liberated from MgATP hydrolysis is not used during stretch but rather during shortening. Such a mechanism would seem energetically and evolutionarily beneficial.

In the model presented in this paper, the nadir of the force response to a quick stretch reflects an enhanced detachment rate caused by stretch. The depth of this nadir, and therefore the energetic savings afforded by the underlying mechanism, is directly dependent on the sensitivity of crossbridge detachment rate to crossbridge displacement, g_1. We expect that this sensitivity constant is defined in part by the amount of deformation experienced by the myosin head and the enhanced probability of power stroke reversal with or without Pi binding. The deformation of the myosin head is further dependent on its mechanical compliance relative to other sarcomeric structures bearing load. The various isoforms, mutations, and phosphorylation statuses of all sarcomeric proteins (actin, titin, myosin-binding protein C, tropomyosin, troponins, etc.) can also modulate the probability of power stroke reversal via their influence on relative sarcomere stiffness, which affects myosin head deformation during stretch. We suspect that slow myosin isoforms provide greater opportunity for power stroke reversal due to the slower MgADP release rate and higher sensitivity to Pi compared with the faster myosin isoforms, as demonstrated in skeletal muscle (Straight et al., 2019). In human cardiac muscle, the slower β-myosin may similarly better suit LV relaxation compared with the faster α-myosin isoform.

Limitations

We have not explained the molecular mechanisms that underlie the power-law relaxation used to fit phase 4. We note that the magnitude of phase 4, measured at t = 1 s, is proportional to crossbridge number as manipulated by MgATP or activating Ca^{2+} concentration. However, at saturating MgATP, the crossbridges that were initially stretched at time 0, modeled as $A_1(t)$, are detached and reattached at new positions within 100 ms and would not directly participate in the elevated stress at t = 1 s. How then can the magnitude of phase 4 be proportional to crossbridge number but not due to the initial stretch of

crossbridges? We speculate the magnitude of phase 4 reflects (a) the transverse stiffness of the sarcomere translated into longitudinal stiffness through Poisson's ratio of the muscle, and (b) the stretched proteins that are in series with the crossbridges, including those that anchor the myofilaments to the M- and Z-lines; both cases would be proportional to crossbridge number and not dependent on those crossbridges initially stretched. Further work is warranted in elucidating the mechanisms underlying phase 4.

Further limitations of the current work include the use of a two-state model of the myosin crossbridge, as stated above, and the use of first-order approximations used throughout our modeling. Of note, we used a constant value for $A_2(t)$ in the model equations of the Supplemental text (see bottom of PDF) that led to the analytical solutions given in Eq. 7. Use of a constant value for $A_2(t)$ linearized the equation and thus permitted a solution. We also used a linear representation for $g(x)$. Such linearization of the equations is warranted when length changes and velocities are small and myosin kinetics and its sensitivity to strain are constant. It is likely, for example, that the rate constants related to transitions from a force-producing state are not strictly linearly related to strain. We must keep in mind that our analytical solutions are useful to characterize myosin kinetics and the strain dependency of the detachment rate only to the extent that our model adequately reflects the underlying processes.

Conclusion

Our findings suggest that phases 2 and 3 of the typical step force response result from a transiently reduced myofilament force caused by a briefly enhanced crossbridge detachment rate with stretch. Furthermore, the elevated force of phase 4 does not necessarily reflect further activation of the thin filament by stretch, but rather a power-law viscoelastic response commonly found in biological tissues. If both these hypotheses are correct, then an enhanced rate of crossbridge detachment with stretch, possibly through a Pi-dependent mechanism, would result in the accelerated relaxation observed with stretch. This stretch-dependent detachment mechanism before MgADP release, if true, could play a significant role in underlying LV diastolic function and dysfunction.

Acknowledgments

Henk L. Granzier served as editor.

This research was supported by grants from the National Institutes of Health (R01 HL-118524, M.M. LeWinter; R01 HL-122744, M. Meyer), the National Institute of Arthritis and Musculoskeletal and Skin Diseases (R01-AR064274, D.M. Swank), the American Heart Association (17SDG33370153, B.C.W. Tanner), and the National Science Foundation (1660908, B.M. Palmer; 1656450, B.C.W. Tanner).

The authors declare no competing financial interests.

Author contributions: All authors participated in conceptualization of the overall topic and in editing the manuscript. B.M. Palmer designed experiments, wrote relevant software, analyzed data, and wrote the original draft. D.M. Swank, M.S. Miller, and M.M. LeWinter interpreted data, provided critical reviews, and curated key references. B.C.W. Tanner collected and curated raw data from mouse myocardium. M. Meyer and M.M. LeWinter provided funds and key resources including laboratory space and human myocardium. All authors approved the final version of the manuscript.

Submitted: 6 September 2019
Revised: 13 January 2020
Accepted: 12 February 2020

References

Baker, J.E., C. Brosseau, P.B. Joel, and D.M. Warshaw. 2002. The biochemical kinetics underlying actin movement generated by one and many skeletal muscle myosin molecules. *Biophys. J.* 82:2134–2147. https://doi.org/10.1016/S0006-3495(02)75560-4

Bell, S.P., L. Nyland, M.D. Tischler, M. McNabb, H. Granzier, and M.M. LeWinter. 2000. Alterations in the determinants of diastolic suction during pacing tachycardia. *Circ. Res.* 87:235–240. https://doi.org/10.1161/01.RES.87.3.235

Brenner, B. 1988. Effect of Ca2+ on crossbridge turnover kinetics in skinned single rabbit psoas fibers: implications for regulation of muscle contraction. *Proc. Natl. Acad. Sci. USA.* 85:3265–3269. https://doi.org/10.1073/pnas.85.9.3265

Campbell, K. 1997. Rate constant of muscle force redevelopment reflects cooperative activation as well as crossbridge kinetics. *Biophys. J.* 72:254–262. https://doi.org/10.1016/S0006-3495(97)78664-8

Campbell, K.B., and M. Chandra. 2006. Functions of stretch activation in heart muscle. *J. Gen. Physiol.* 127:89–94. https://doi.org/10.1085/jgp.200509483

Chung, C.S., C.W. Hoopes, and K.S. Campbell. 2017. Myocardial relaxation is accelerated by fast stretch, not reduced afterload. *J. Mol. Cell. Cardiol.* 103:65–73. https://doi.org/10.1016/j.yjmcc.2017.01.004

Dantzig, J.A., Y.E. Goldman, N.C. Millar, J. Lacktis, and E. Homsher. 1992. Reversal of the crossbridge force-generating transition by photogeneration of phosphate in rabbit psoas muscle fibres. *J. Physiol.* 451:247–278. https://doi.org/10.1113/jphysiol.1992.sp019163

Debold, E.P., S. Walcott, M. Woodward, and M.A. Turner. 2013. Direct observation of phosphate inhibiting the force-generating capacity of a miniensemble of Myosin molecules. *Biophys. J.* 105:2374–2384. https://doi.org/10.1016/j.bpj.2013.09.046

Djordjević, V.D., J. Jarić, B. Fabry, J.J. Fredberg, and D. Stamenović. 2003. Fractional derivatives embody essential features of cell rheological behavior. *Ann. Biomed. Eng.* 31:692–699. https://doi.org/10.1114/1.1574026

Donaldson, C., B.M. Palmer, M. Zile, D.W. Maughan, J.S. Ikonomidis, H. Granzier, M. Meyer, P. VanBuren, and M.M. LeWinter. 2012. Myosin crossbridge dynamics in patients with hypertension and concentric left ventricular remodeling. *Circ. Heart Fail.* 5:803–811. https://doi.org/10.1161/CIRCHEARTFAILURE.112.968925

Dunlay, S.M., V.L. Roger, and M.M. Redfield. 2017. Epidemiology of heart failure with preserved ejection fraction. *Nat. Rev. Cardiol.* 14:591–602. https://doi.org/10.1038/nrcardio.2017.65

Fujita, H., and M. Kawai. 2002. Temperature effect on isometric tension is mediated by regulatory proteins tropomyosin and troponin in bovine myocardium. *J. Physiol.* 539:267–276. https://doi.org/10.1113/jphysiol.2001.013220

Fujita, H., D. Sasaki, S. Ishiwata, and M. Kawai. 2002. Elementary steps of the crossbridge cycle in bovine myocardium with and without regulatory proteins. *Biophys. J.* 82:915–928. https://doi.org/10.1016/S0006-3495(02)75453-2

Gong, H., V. Hatch, L. Ali, W. Lehman, R. Craig, and L.S. Tobacman. 2005. Mini-thin filaments regulated by troponin-tropomyosin. *Proc. Natl. Acad. Sci. USA.* 102:656–661. https://doi.org/10.1073/pnas.0407225102

Houdusse, A., and H.L. Sweeney. 2001. Myosin motors: missing structures and hidden springs. *Curr. Opin. Struct. Biol.* 11:182–194. https://doi.org/10.1016/S0959-440X(00)00188-3

Huxley, A.F. 1957. Muscle structure and theories of contraction. *Prog. Biophys. Biophys. Chem.* 7:255–318. https://doi.org/10.1016/S0096-4174(18)30128-8

Kad, N.M., J.B. Patlak, P.M. Fagnant, K.M. Trybus, and D.M. Warshaw. 2007. Mutation of a conserved glycine in the SH1-SH2 helix affects the

load-dependent kinetics of myosin. *Biophys. J.* 92:1623–1631. https://doi.org/10.1529/biophysj.106.097618

Kass, D.A., J.G. Bronzwaer, and W.J. Paulus. 2004. What mechanisms underlie diastolic dysfunction in heart failure? *Circ. Res.* 94:1533–1542. https://doi.org/10.1161/01.RES.0000129254.25507.d6

Kawai, M., and P.W. Brandt. 1980. Sinusoidal analysis: a high resolution method for correlating biochemical reactions with physiological processes in activated skeletal muscles of rabbit, frog and crayfish. *J. Muscle Res. Cell Motil.* 1:279–303. https://doi.org/10.1007/BF00711932

Kawai, M., and S. Ishiwata. 2006. Use of thin filament reconstituted muscle fibres to probe the mechanism of force generation. *J. Muscle Res. Cell Motil.* 27:455–468. https://doi.org/10.1007/s10974-006-9075-4

Liu, C., M. Kawana, D. Song, K.M. Ruppel, and J.A. Spudich. 2018. Controlling load-dependent kinetics of β-cardiac myosin at the single-molecule level. *Nat. Struct. Mol. Biol.* 25:505–514. https://doi.org/10.1038/s41594-018-0069-x

Lu, X., M.K. Bryant, K.E. Bryan, P.A. Rubenstein, and M. Kawai. 2005. Role of the N-terminal negative charges of actin in force generation and crossbridge kinetics in reconstituted bovine cardiac muscle fibres. *J. Physiol.* 564:65–82. https://doi.org/10.1113/jphysiol.2004.078055

Mansfield, C., T.G. West, N.A. Curtin, and M.A. Ferenczi. 2012. Stretch of contracting cardiac muscle abruptly decreases the rate of phosphate release at high and low calcium. *J. Biol. Chem.* 287:25696–25705. https://doi.org/10.1074/jbc.M112.373498

Moss, R.L., M. Razumova, and D.P. Fitzsimons. 2004. Myosin crossbridge activation of cardiac thin filaments: implications for myocardial function in health and disease. *Circ. Res.* 94:1290–1300. https://doi.org/10.1161/01.RES.0000127125.61647.4F

Palmer, B.M., T. Suzuki, Y. Wang, W.D. Barnes, M.S. Miller, and D.W. Maughan. 2007. Two-state model of acto-myosin attachment-detachment predicts C-process of sinusoidal analysis. *Biophys. J.* 93:760–769. https://doi.org/10.1529/biophysj.106.101626

Palmer, B.M., B.C. Tanner, M.J. Toth, and M.S. Miller. 2013. An inverse power-law distribution of molecular bond lifetimes predicts fractional derivative viscoelasticity in biological tissue. *Biophys. J.* 104:2540–2552. https://doi.org/10.1016/j.bpj.2013.04.045

Perz-Edwards, R.J., T.C. Irving, B.A. Baumann, D. Gore, D.C. Hutchinson, U. Kržič, R.L. Porter, A.B. Ward, and M.K. Reedy. 2011. X-ray diffraction evidence for myosin-troponin connections and tropomyosin movement during stretch activation of insect flight muscle. *Proc. Natl. Acad. Sci. USA.* 108:120–125. https://doi.org/10.1073/pnas.1014599107

Ranatunga, K.W. 1999. Effects of inorganic phosphate on endothermic force generation in muscle. *Proc. Biol. Sci.* 266:1381–1385. https://doi.org/10.1098/rspb.1999.0791

Runte, K.E., S.P. Bell, D.E. Selby, T.N. Häußler, T. Ashikaga, M.M. LeWinter, B.M. Palmer, and M. Meyer. 2017. Relaxation and the role of calcium in isolated contracting myocardium from patients with hypertensive heart disease and heart failure with preserved ejection fraction. *Circ. Heart Fail.* 10:e004311. https://doi.org/10.1161/CIRCHEARTFAILURE.117.004311

Selby, D.E., B.M. Palmer, M.M. LeWinter, and M. Meyer. 2011. Tachycardia-induced diastolic dysfunction and resting tone in myocardium from patients with a normal ejection fraction. *J. Am. Coll. Cardiol.* 58:147–154. https://doi.org/10.1016/j.jacc.2010.10.069

Sequeira, V., A. Najafi, M. McConnell, E.D. Fowler, I.A. Bollen, R.C. Wüst, C. dos Remedios, M. Helmes, E. White, G.J. Stienen, et al. 2015. Synergistic role of ADP and Ca(2+) in diastolic myocardial stiffness. *J. Physiol.* 593:3899–3916. https://doi.org/10.1113/JP270354

Smith, D.A., and M.A. Geeves. 1995. Strain-dependent crossbridge cycle for muscle. II. Steady-state behavior. *Biophys. J.* 69:538–552. https://doi.org/10.1016/S0006-3495(95)79927-1

Stelzer, J.E., and R.L. Moss. 2006. Contributions of stretch activation to length-dependent contraction in murine myocardium. *J. Gen. Physiol.* 128:461–471. https://doi.org/10.1085/jgp.200609634

Straight, C.R., K.M. Bell, J.N. Slosberg, M.S. Miller, and D.M. Swank. 2019. A myosin-based mechanism for stretch activation and its possible role revealed by varying phosphate concentration in fast and slow mouse skeletal muscle fibers. *Am. J. Physiol. Cell Physiol.* 317:C1143–C1152. https://doi.org/10.1152/ajpcell.00206.2019

Tyska, M.J., and D.M. Warshaw. 2002. The myosin power stroke. *Cell Motil. Cytoskeleton.* 51:1–15. https://doi.org/10.1002/cm.10014

Veigel, C., S. Schmitz, F. Wang, and J.R. Sellers. 2005. Load-dependent kinetics of myosin-V can explain its high processivity. *Nat. Cell Biol.* 7:861–869. https://doi.org/10.1038/ncb1287

Zhang, J., J. Chen, B. Cheong, A. Pednekar, and R. Muthupillai. 2019. High frame rate cardiac cine MRI for the evaluation of diastolic function and its direct correlation with echocardiography. *J. Magn. Reson. Imaging.* 50:1571–1582. https://doi.org/10.1002/jmri.26791

Zhao, C., and D.M. Swank. 2013. An embryonic myosin isoform enables stretch activation and cyclical power in Drosophila jump muscle. *Biophys. J.* 104:2662–2670. https://doi.org/10.1016/j.bpj.2013.04.057

Zile, M.R., and W.H. Gaasch. 1991. Load-dependent left ventricular relaxation in conscious dogs. *Am. J. Physiol.* 261:H691–H699.

Zile, M.R., C.F. Baicu, J.S. Ikonomidis, R.E. Stroud, P.J. Nietert, A.D. Bradshaw, R. Slater, B.M. Palmer, P. Van Buren, M. Meyer, et al. 2015. Myocardial stiffness in patients with heart failure and a preserved ejection fraction: contributions of collagen and titin. *Circulation.* 131:1247–1259. https://doi.org/10.1161/CIRCULATIONAHA.114.013215

Supplemental material

This supplement provides a detailed derivation of the mathematical model we use to describe the consequences of strain-dependent myosin crossbridge kinetics on the recorded force response of muscle to a quick stretch. We refer to figures in the main text when necessary.

The conceptual model we consider here is a two-state model in which the myosin head is in either a strongly bound force-producing state or a weakly bound non–force-producing state. These two states are also referred to as attached (A) and detached (D) to the thin filament as illustrated in Fig. 4 B. The attachment and detachment rate constants are functions of length x, $f(x)$, and $g(x)$, although defined differently from those functions first proposed by Huxley (1957).

In the differential equation developed below, $A(x,t)$ represents the spatial and temporal distribution of the fraction of the myosin heads in the attached state. The spatial distribution of newly formed strongly bound crossbridges is given by $f(x)$, which we assume here to be symmetrical about $x = 0$, and represents the myosin binding site on the thin filament relative to a nondisplaced myosin head emanating from the thick filament (Fig. 4 B). We also include an explicit strain dependence on the detachment rate, $g(x) = g_0 + g_1x$. The term g_0 represents the rate constant when there is no external strain imposed on the crossbridge adding to that caused by the power stroke. The term g_1 represents the linear sensitivity of detachment rate to the strain experienced by attached crossbridges along the x dimension. The positive sign associated with g_1 signifies that detachment rate $g(x)$ is enhanced with muscle lengthening and reduced with shortening.

The differential equation describing the change in the fraction of myosin heads attached is

$$\frac{dA(x,t)}{dt} = f(x)\left[1 - \int_{-\infty}^{\infty} A(x,t)dx\right] - g(x)A(x,t), \quad \text{(S1)}$$

where the bracketed term

$$\left[1 - \int_{-\infty}^{\infty} A(x,t)dx\right]$$

represents the fraction of myosin in the detached state at any time t.

There are two modifications that must be made to Eq. S1. First, the attached state is subject to length displacement due to movement of the thin filament relative to the thick filament. Therefore, the derivative with respect to time is subject to the chain rule:

$$\frac{dA(x,t)}{dt} = \frac{\partial A(x,t)}{\partial t} + v(t)\frac{\partial A(x,t)}{\partial x}, \quad \text{(S2)}$$

where $v(t)$ is the velocity, $dx(t)/dt$, of any displacement of a myosin head relative to the thick filament caused by movement of the thin filament, as would occur with an externally driven length perturbation. Second, instead of solving Eq. S1, which is a partial differential equation in two dimensions, we solve for the spatial moments of $A(x,t)$ along the x axis, thus simplifying the model into a set of ordinary differential equations in one dimension. Specifically, we will take the following integration over the x dimension,

$$\int_{-\infty}^{\infty} x^m (\text{Eq. S1})dx,$$

where m = an integer defining the moments of a distribution.

We make the following definitions to facilitate our development:

$$\int_{-\infty}^{\infty} x^m A(x,t)dx = A_m(t), \quad \text{(S3a)}$$

$$\int_{-\infty}^{\infty} x^m \frac{\partial A(x,t)}{\partial x}dx = [x^m A(x,t)]\Big|_{-\infty}^{\infty} - \int_{-\infty}^{\infty} m x^{m-1} A(x,t)dx = -mA_{m-1}(t), \quad \text{(S3b)}$$

and

$$\int_{-\infty}^{\infty} x^m f(x)dx = f_m. \quad \text{(S3c)}$$

Upon applying the chain rule of Eq. S2 and the moments defined in Eq. S3, Eq. S1 becomes

$$\frac{dA_m(t)}{dt} = mv(t)A_{m-1}(t) + f_m[1 - A_0(t)] - g_0A_m(t) - g_1A_{m+1}(t). \quad \text{(S4)}$$

Eq. S4 represents a series of equations for different values of m. When $m = 0$, Eq. S4 describes the fraction of crossbridges in the attached state. When $m = 1$, Eq. S4 describes the mean displacement of the crossbridges in the attached state. When $m = 2$, Eq. S4 is

proportional to the variance of crossbridge displacement. We solve Eq. S4 for $m = 0$ and 1, which directly relate to the myosin unitary force and the force due to strain on the myosin crossbridge, respectively.

Steady-state solutions

When there is no length perturbation and no change in A_m, the velocity $v(t) = 0$, and the time derivative

$$\frac{dA(x,t)}{dt} = 0,$$

Eq. S4 reduces to the following:

$$0 = f_m(1 - \bar{A}_0) - g_0\bar{A}_m - g_1\bar{A}_{m+1}, \quad \text{(S5a)}$$

or equivalently,

$$\bar{A}_m = \frac{f_m}{g_0}(1 - \bar{A}_0) - \frac{g_1}{g_0}\bar{A}_{m+1}, \quad \text{(S5b)}$$

where the bar signifies the steady-state condition. Because of the even symmetry of $f(x)$ about $x = 0$, f_m will equal 0 for odd values of m. Furthermore, we assume that $\bar{A}_m$ are negligible for $m \geq 3$. For $m = 0$, 1, and 2, the steady-state equations are

$$\bar{A}_0 = \frac{f_0}{g_0}(1 - \bar{A}_0) - \frac{g_1}{g_0}\bar{A}_1, \quad \text{(S6a)}$$

$$\bar{A}_1 = -\frac{g_1}{g_0}\bar{A}_2, \quad \text{(S6b)}$$

and

$$\bar{A}_2 = \frac{f_2}{g_0}(1 - \bar{A}_0). \quad \text{(S6c)}$$

The steady-state solutions are

$$\bar{A}_0 = \frac{f_0 + f_2(g_1/g_0)^2}{(f_0 + g_0) + f_2(g_1/g_0)^2}, \quad \text{(S7a)}$$

$$\bar{A}_1 = \frac{-f_2(g_1/g_0)}{(f_0 + g_0) + f_2(g_1/g_0)^2}, \quad \text{(S7b)}$$

and

$$\bar{A}_2 = \frac{f_2}{(f_0 + g_0) + f_2(g_1/g_0)^2}. \quad \text{(S7c)}$$

The expressions in Eq. S7 account for the strain dependence described in $g(x)$. If there were no strain dependence, i.e., if $g_1 = 0$, the fraction of attached crossbridges $\bar{A}_0$ would reduce to $f_0/(f_0 + g_0)$, and the mean displacement $\bar{A}_1$ would be 0. With strain dependence, i.e., $g_1 > 0$, the mean steady-state displacement of the attached crossbridges $\bar{A}_1$ is negative, due to the reduced detachment rate with compression ($x < 0$) and enhanced detachment rate with stretch ($x > 0$).

Mean displacement of attached crossbridges, $m = 1$

For $m = 1$, Eq. S4 is nonlinear due to the product of two functions of time, $v(t)$ and $A_0(t)$. To achieve an analytical solution for Eq. S4, we linearize the expression. We assume that, for very small perturbations, the steady-state value $\bar{A}_0$ suitably approximates $A_0(t)$ in the velocity-dependent term. We also recall $f_1 = 0$, which removes the f_1 term. We further assume that $\bar{A}_2$ suitably approximates $A_2(t)$ in the last term. Eq. S4 for $m = 1$ is then written as

$$\frac{dA_1(t)}{dt} = v(t)\bar{A}_0 - g_0A_1(t) - g_1\bar{A}_2. \quad \text{(S8)}$$

The linear operator Laplace transform is useful for solving differential equations with constant coefficients and can be applied to Eq. S8 to provide an equation in the frequency domain with complex variable, s. For a length perturbation of the half sarcomere, $L(t) + L_{hs}$, in units of nm, where L_{hs} is the resting half-sarcomere length maintained until $t = 0$, the Laplace transform of $v(t)$ is $s\tilde{L}(s)$, and the equation in full becomes

$$s\tilde{A}_1(s) - \bar{A}_1 = s\tilde{L}(s)\bar{A}_0 - g_0\tilde{A}_1(s) - s^{-1}g_1\bar{A}_2, \quad \text{(S9)}$$

and

$$(s + g_0)\tilde{A}_1(s) = \bar{A}_1 + s\tilde{L}(s)\bar{A}_0 - s^{-1}g_1\bar{A}_2. \quad \text{(S10)}$$

Using Eq. S6b, we substitute $\bar{A}_2$ with $-(g_0/g_1)\bar{A}_1$ and simplify the terms. The solution is

$$\tilde{A}_1(s) = s^{-1}\bar{A}_1 + \frac{\bar{A}_0}{(s + g_0)}s\tilde{L}(s). \quad \text{(S11)}$$

Eq. S11 represents the mean displacement of myosin crossbridges in frequency space. Its response to a step-length change of ΔL in the half-sarcomere is calculated by substituting $\tilde{L}(s)$ in Eq. S11 with the Laplace representation of this step-length change, $\Delta L s^{-1}$, and then solving the inverse Laplace transform:

$$A_1(t) = \bar{A}_1 + \Delta L\bar{A}_0 e^{-g_0 t} \quad \text{for } t \geq 0, \quad \text{(S12)}$$

where $e^{-g_0 t}$ = exponential function with a decay rate g_0 s^{-1}. In practice, ΔL is ≤1% of the resting half-sarcomere length, i.e., ≤10 nm for a half sarcomere of ∼1 µm, to best ensure a linear response. An example $A_1(t)$ for 10-nm stretch is shown in Fig. 5 B. The expected force due to displacement of myosin crossbridges, $F_1(t)$, requires the multiplication of Eq. S12 by N_{hs}, the total number of available myosin crossbridges in a half-sarcomere, and k_{stiff}, the stiffness of each crossbridge with units pN · nm^{-1}:

$$F_1(t) = N_{hs}k_{stiff}\bar{A}_1 + \Delta L N_{hs}k_{stiff}\bar{A}_0 e^{-g_0 t} \quad \text{for } t \geq 0. \quad \text{(S13)}$$

Furthermore, the stress due to displacement of attached crossbridges, $\sigma_1(t)$, is calculated by normalizing $F_1(t)$ to cross-sectional area of the muscle sample, CSA. We use the resting half-sarcomere length, L_{hs}, to normalize ΔL and define strain, $\varepsilon = \Delta L/L_{hs}$, imposed on the muscle during the step-length change:

$$\sigma_1(t) = \lambda\bar{A}_1 + \varepsilon L_{hs}\lambda\bar{A}_0 e^{-g_0 t} \quad \text{for } t \geq 0, \quad \text{(S14)}$$

where

$$\lambda = \frac{N_{hs}k_{stiff}}{CSA}$$

with units pN · mm^{-2} · nm^{-1}, and the product $L_{hs}\lambda$ represents the mean elastic modulus of any available crossbridge in units pN · mm^{-2}. An example $\sigma_1(t)$ is also shown in Fig. 5 B.

Fraction of crossbridges attached, m = 0

We now apply the above result for the $A_1(t)$ in Eq. S12 to demonstrate the consequences of a length dependence of myosin detachment rate on the fraction of crossbridges attached. We solve Eq. S4 for the case m = 0:

$$\frac{dA_0(t)}{dt} = f_0[1 - A_0(t)] - g_0A_0(t) - g_1A_1(t). \quad \text{(S15)}$$

Laplace transform produces

$$s\tilde{A}_0(s) - \bar{A}_0 = f_0[s^{-1} - \tilde{A}_0(s)] - g_0\tilde{A}_0(s) - g_1\tilde{A}_1(s). \quad \text{(S16)}$$

We arrange all $\tilde{A}_0(s)$ on the left, use the term for $\tilde{A}_1(s)$ given in Eq. S11, and solve for $\tilde{A}_0(s)$:

$$(s + f_0 + g_0)\tilde{A}_0(s) = \bar{A}_0 + s^{-1}f_0 - g_1\tilde{A}_1(s), \quad \text{(A17)}$$

$$(s + f_0 + g_0)\tilde{A}_0(s) = \bar{A}_0 + s^{-1}f_0 - g_1\left[s^{-1}\bar{A}_1 + \frac{s\bar{A}_0}{(s + g_0)}\tilde{L}(s)\right], \quad \text{(S18)}$$

and

$$\tilde{A}_0(s) = \frac{\bar{A}_0 + s^{-1}f_0 - g_1s^{-1}\bar{A}_1}{(s + f_0 + g_0)} - \frac{g_1s\bar{A}_0}{(s + f_0 + g_0)(s + g_0)}\tilde{L}(s). \quad \text{(S19)}$$

We now substitute f_0 in the first term with $\bar{A}_0[(f_0 + g_0) + f_2(g_1/g_0)^2] - f_2(g_1/g_0)^2$ based on Eq. S7a, and we substitute $\bar{A}_1$ with

$$\frac{-f_2g_1}{{g_0}^2}[1 - \bar{A}_0]$$

from Eq. S6. Many parts in the numerator of the first term then cancel each other, and we are left with

$$\tilde{A}_0(s) = \frac{s\bar{A}_0 + (f_0 + g_0)\bar{A}_0}{s(s + f_0 + g_0)} - \frac{g_1 s\bar{A}_0}{(s + f_0 + g_0)(s + g_0)}\tilde{L}(s), \quad \text{(S20)}$$

and

$$\tilde{A}_0(s) = s^{-1}\bar{A}_0 - \frac{g_1\bar{A}_0}{(s + f_0 + g_0)(s + g_0)}s\tilde{L}(s). \quad \text{(S21)}$$

Finally, the solution for $\tilde{A}_0(s)$ is equivalently given as

$$\tilde{A}_0(s) = s^{-1}\bar{A}_0 - g_1\bar{A}_0\left[\frac{f_0^{-1}}{(s + g)} - \frac{f_0^{-1}}{(s + f_0 + g)}\right]s\tilde{L}(s). \quad \text{(S22)}$$

To the extent that our model and its explicit and implicit assumptions are reasonable reflections of the molecular-level physiology, the fraction of myosin heads attached in response to a small step-length change of ΔL would have the following form:

$$A_0(t) = \bar{A}_0 - \Delta L\frac{g_1\bar{A}_0}{f_0}\left(e^{-g_0 t} - e^{-(f_0+g_0)t}\right). \quad \text{(S23)}$$

The result in Eq. S23 describes a transient reduction in the fraction of force-producing myosin crossbridges attached after a step-length change (Fig. 5 C). The g_0-exponential term describes the new equilibration point for the fraction of crossbridges attached due to strain imposed on them, and the $(f_0 + g_0)$-exponential term represents the rate of reequilibration in a two-state model (Brenner, 1988).

The force attributable to this fraction of myosin crossbridges would require the multiplication of N_{hs}, the total number of available myosin crossbridges in a half-sarcomere, and F_{uni}, the unitary force produced by each myosin crossbridge, in units of pN.

$$F_0(t) = N_{hs}F_{uni}\bar{A}_0 - \Delta L N_{hs}F_{uni}\frac{g_1\bar{A}_0}{f_0}\left(e^{-g_0 t} - e^{-(f_0+g_0)t}\right) \quad \text{for } t \geq 0. \quad \text{(S24)}$$

The stress due to the fraction of myosin crossbridge attached, $\sigma_0(t)$, requires normalizing to CSA:

$$\sigma_0(t) = \gamma\bar{A}_0 - \varepsilon L_{hs}\gamma\frac{g_1\bar{A}_0}{f_0}\left(e^{-g_0 t} - e^{-(f_0+g_0)t}\right) \quad \text{for } t \geq 0, \quad \text{(S25)}$$

where

$$\gamma = \frac{N_{hs}F_{uni}}{CSA}$$

with units of pN · mm^{-2} represents the active stress generated by myosin crossbridges in the half-sarcomere. An example $\sigma_0(t)$ is also shown in Fig. 5 C.